

THESIS FOR THE DEGREE OF DOCTOR OF PHILOSOPHY

**Synthesis and Modification of Conjugated Materials for  
Polymer Solar Cells**

ZANDRA GEORGE



Department of Chemistry and Chemical Engineering

CHALMERS UNIVERSITY OF TECHNOLOGY

Gothenburg, Sweden 2016

# **SYNTHESIS AND MODIFICATION OF CONJUGATED MATERIALS FOR POLYMER SOLAR CELLS**

ZANDRA GEORGE

© ZANDRA GEORGE, 2016  
ISBN 978-91-7597-345-6

Doktorsavhandlingar vid Chalmers tekniska högskola  
Ny serie nr 4026  
ISSN 0346-718X

Division of Applied Chemistry  
Department of Chemistry and Chemical Engineering  
Chalmers University of Technology  
SE-412 96 Gothenburg  
Sweden  
Telephone + 46 (0) 31-772 10 00

Cover:  
Photoluminescence of polyfluorene in solution.  
Photo by Zandra George and Renee Kroon

Chalmers Reproservice  
Gothenburg, Sweden 2016

# Synthesis and Modification of Conjugated Materials for Polymer Solar Cells

ZANDRA GEORGE

*Department of Chemistry and Chemical Engineering*

Chalmers University of Technology

Gothenburg, Sweden

## ABSTRACT

---

Polymer solar cells have emerged as a promising alternative to silicon based solar cells. One of the advantages of polymer solar cells is the possibility to use roll-to-roll techniques for large-scale device production. However, in order to fully utilize this technique, several issues need to be resolved. The bottom electrodes of large-area devices are one critical aspect that typically requires modification with interlayers in order to achieve high performance. The main focus of this thesis has been on the design, synthesis and evaluation of such interfacial materials.

In the first part of the thesis, a well performing DPP-based polymer was modified with alkoxy side chains to investigate the effect of various polymer properties. In addition to a redshift in the absorption, other polymer properties were altered, proposing increased flexibility in the polymer chain.

The effect of adding an ultrathin layer of an amine-functionalized conjugated polymer between the cathode and active layer in polymer solar cells is studied using four different interlayer polymers. The introduction of these interlayer polymers to the device structure resulted in enhanced solar cell performance due to an improvement in surface and electrical properties of the substrate electrode. In addition, the polymers also improve the photo-stability of devices, mainly as an effect of a reduced decrease in open-circuit voltage and fill factor.

Finally, two fullerene derivatives were used to simultaneously achieve both work function modification of the electrode and improved thermal stability of polymer

solar cells. The use of fullerene interlayers resulted in higher photovoltaic performance. Moreover, the photovoltaic performance is retained in polymer solar cell blends that otherwise rapidly deteriorate at elevated temperatures.

**Keywords:** *polymer solar cells, conjugated polymers, polymer interlayer, stability, fullerene derivatives*

# LIST OF PUBLICATIONS

---

This thesis is based on the following scientific papers, referred to by their roman numerals in the text. The papers are appended at the end of the thesis.

**Paper I. Interlayer for Modified Cathode in Highly Efficient Inverted ITO-Free Organic Solar Cells**

Zheng Tang; Mattias L. Andersson; Zandra George; Koen Vandewal; Kristofer Tvingstedt; Patrik Henriksson; Renee Kroon; Mats R. Andersson; Olle Inganäs  
*Advanced Materials*, 2012, 24(4), 554-558

**Paper II. The influence of alkoxy substitutions on the properties of diketopyrrolopyrrole-phenyl copolymers for solar cells**

Zandra George; Renee Kroon; Robert Gehlhaar; Gabin Gbabode; Angelica Lundin; Stefan Hellström; Christian Müller; Yves Geerts; Paul Heremans; Mats R.  
*Materials*, 2013, 6, 3022-3034

**Paper III. Improved performance and life time of inverted organic photovoltaics by using polymer interfacial materials**

Zandra George; Eszter Voroshazi; Camilla Lindqvist; Renee Kroon; Wenliu Zhuang; Ergang Wang; Patrik Henriksson; Afshin Hadipour; Mats R Andersson  
*Solar Energy Materials and Solar Cells*, 2015, 133c. 99-104

**Paper IV. Two-in-One: Cathode modification and improved solar cell blend stability through addition of modified fullerenes**

Zandra George; Yuxin Xia; Anirudh Sharma; Camilla Lindqvist; Gunther Andersson; Olle Inganäs; Ellen Moons; Christian Müller; Mats R. Andersson  
*Journal of Materials Chemistry A*, 2016, 4, 2663 - 2669

Paper V. **Stability of Polymer Interlayer Modified ITO Electrodes for Organic Solar Cells**

Anirudh Sharma; Zandra George; Trystan Bennett; David A. Lewis; Gregory F. Metha; Gunther Andersson; Mats R. Andersson

*Accepted in Australian Journal of Chemistry, 2016*

# CONTRIBUTION REPORT

---

- Paper I.** Synthesis and characterization of PFPA-1 and its intermediates, some writing.
- Paper II.** Synthesis of P2, P3 and the organic intermediates. Some of the physical and optical characterization. Responsible for part of the interpretation of the results and writing the manuscript with input from my co-authors.
- Paper III.** Synthesis and characterization of the polymers. Interpretation of most results and writing the manuscript with input from my co-authors.
- Paper IV.** Synthesis and characterization of the PCBM derivatives. Interpretation of results together with my co-authors and writing the manuscript with input from my co-authors.
- Paper V.** Synthesis and characterization of the polymers and its intermediates.

## **PUBLICATIONS NOT INCLUDED IN THE THESIS**

---

Paper VI. **Semi-transparent tandem organic solar cells with 90% internal quantum efficiency**

Zheng Tang; Zandra George; Zaifei Ma; Jonas Bergqvist; Kristofer Tvingstedt; Koen Vandewal; Ergang Wang; Mattias L. Andersson, Mats R. Andersson; Fengling Zhang, Olle Inganäs

*Advanced Energy Materials* (2012), 2(12), 1467-1476

Paper VII. **Stability study of quinoxaline and pyrido pyrazine based co-polymers for solar cell applications**

Patrik Henriksson; Camilla Lindqvist; Bedasa Abdisa; Ergang Wang; Zandra George; Renee Kroon; Christian Müller, Teketel Yohannes; Olle Inganäs; Mats R. Andersson

*Solar Energy Materials & Solar Cells* (2014), 130, 138-143

## ABBREVIATIONS AND ACRONYMS

---

AFM	Atomic Force Microscopy
BHJ	Bulk-heterojunction
DSC	Differential Scanning Calorimetry
EQE	External Quantum Efficiency
FF	Fill Factor
HOMO	Highest Occupied Molecular Orbital
iFSC	Inverted ITO-free solar cell
iPSC	Inverted Polymer Solar Cell
ITO	Indium Tin Oxide
$J_{sc}$	Short Circuit Current Density
LUMO	Lowest Unoccupied Molecular Orbital
MALDI-TOF	Matrix-Assisted Laser Desorption/Ionization Time-of-flight
MIES	Metastable Induced Electron Spectroscopy
MPP	Maximum Power Point
$\eta$	Efficiency
PCE	Power Conversion Efficiency
PSC	Polymer Solar Cell
SEM	Scanning Electron Microscopy
SWV	Square Wave Voltammetry
TGA	Thermogravimetric Analysis
UPS	Ultraviolet Photoelectron Spectroscopy
$V_{oc}$	Open Circuit Voltage

# TABLE OF CONTENTS

---

---

<b>1 INTRODUCTION.....</b>	<b>1</b>
<b>2 POLYMER SOLAR CELLS .....</b>	<b>5</b>
2.1 Background .....	5
2.2 Conjugated polymers .....	6
2.3 Fullerene derivatives .....	8
2.4 Device architecture.....	9
2.5 Working principle of polymer solar cells .....	11
2.6 IV-characteristics .....	12
2.7 Polymerization reactions .....	13
2.7.1 Suzuki cross-coupling polymerization.....	14
2.7.2 Stille cross-coupling polymerization .....	14
<b>3 DIKETOPYRROLOPYRROLE-BASED POLYMERS .....</b>	<b>17</b>
3.1 Introduction .....	17
3.2 Synthesis .....	18
3.3 Physical and optical properties.....	19
3.4 Photovoltaic performance .....	21
<b>4 POLYMER INTERLAYERS .....</b>	<b>23</b>
4.1 Introduction.....	23
4.2 ITO free inverted polymer solar cells.....	25
4.2.1 Synthesis.....	25
4.2.2 Energy levels.....	26
4.2.3 Photovoltaic performance .....	27
4.2.4 Surface modification .....	28

4.3 Influence on device stability .....	30
4.3.1 <i>Synthesis</i> .....	30
4.3.2 <i>Energy levels</i> .....	31
4.3.3 <i>Polymer stability</i> .....	32
4.3.4 <i>Photovoltaic performance and life time</i> .....	34
4.3.5 <i>Electrode stability</i> .....	36
<b>5 FULLERENE DERIVATIVES.....</b>	<b>39</b>
5.1 Introduction .....	39
5.2 Synthesis .....	41
5.3 Surface modification .....	42
5.3 Blend nanostructure and thermal stability .....	43
5.4 Photovoltaic performance .....	54
<b>6 CONCLUDING REMARKS.....</b>	<b>58</b>
<b>ACKNOWLEDGEMENTS.....</b>	<b>62</b>
<b>REFERENCES.....</b>	<b>65</b>



# 1 INTRODUCTION

The global energy demand is increasing, especially in fast developing countries with a large population such as China and India (Figure 1.1). Today, the world power consumption amounts to around 16 TW globally. A majority of the consumed energy is generated by fossil fuels which include oil, coal and natural gas and only a minor part is generated from renewable energy sources. In order to stop the worldwide increase in energy use and reach a sustainable society where everyone can have a high life standard, some parts of the world has to decrease their energy consumption. To achieve this, the European Union (EU), as well as individual governments, has set goals regarding future energy production and consumption. Until 2020 the EU is aiming to reduce both Europe's annual primary energy consumption and the emission of greenhouse gases (i.e. carbon dioxide, nitrogen oxides, methane etc.) by 20 %. [1] The focus will mainly be at the public transport and building sectors where the potential for savings is the highest.

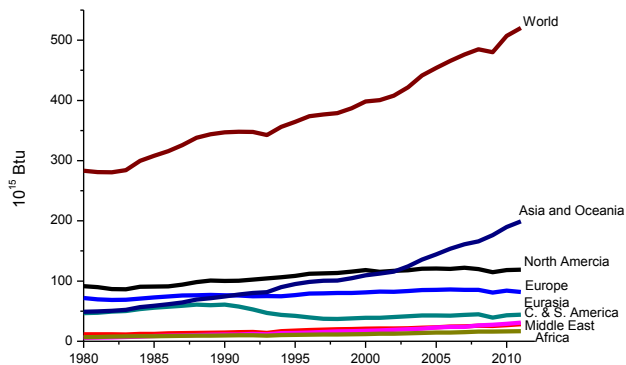


Figure 1.1: World energy consumption from 1980 to 2012 according to the U.S. Energy Information Administration[2]

There is a growing demand for sustainable energy sources. The term “sustainable” refers to that these energy sources should be renewable as well as not increasing the

amount of greenhouse gases in the atmosphere (CO<sub>2</sub>-neutral). Energy sources that fulfill these demands are wind power, geothermal energy, hydroelectric power, wave power, biomass-based energy and solar energy.

The energy that Earth receives from the sun would be more than enough to cover the energy demand of the planet. Solar cells of different types have gained a lot of interest during the last decades. Today, the most commonly used solar cell technique is silicon based. This type of solar cell offers high power conversion efficiency (PCE) of 25 % on lab scale and 11–16 % in commercial arrays and life times of about 20 years. [3] But even though silicon is an abundant and cheap material the requirement of high purity and thick silicon-layers makes this type of solar cells relatively expensive. Therefore, there is a need for alternative solar energy technologies and a lot of research efforts have been put into this area.

Organic thin-film solar cell technologies e.g. polymer solar cells (PSCs) have been shown to be a promising alternative to the silicon-based solar cells. Normally, polymers are regarded as insulators, unable to conduct electricity or absorb sun light. However, in 1977 Shirakawa, McDiarmid and Heeger published a work where polyacetylene (PA) doped with iodine resulted in maximum conductivities of approximately 38 S cm<sup>-1</sup>. [4] For their discovery and contribution to development of conjugated polymers; Shirakawa, McDiarmid and Heeger were awarded the Nobel Prize in chemistry in 2000. [5] Their work opened up for the research of conjugated polymers as the semiconducting material in solar cells, light-emitting diodes and field-effect transistors. The main advantage of PSCs is the potential of flexible and light-weight devices that can be solution processed by cheap and efficient methods such as roll-to-roll processing, inkjet printing or spray coating. Nowadays, the efficiency of lab-scale devices is ~9-10 %. [6-8] However, in order to compete with silicon based solar cells and other energy sources the relatively low stability and short life time of PSCs have to be improved.

The work described in this thesis includes the design, synthesis and characterization of conjugated polymers and fullerene derivatives for polymer solar cells. The

## Introduction

structure-property relationship is investigated for polymers in the active layer of the solar cell as well as for interlayer polymers in solar cells with inverted structure. The stability and morphological effect by addition of interlayer polymers or fullerene derivatives have also been studied.

The synthesis and characterization has been done at Chalmers University of Technology, Sweden, while device characterization has been performed in collaboration with the group of Olle Inganäs at Linköping University, Sweden and at IMEC, Belgium. This work has been funded by the EU-project ONE-P under grant no. 212311 and the Swedish Energy Agency.

## Introduction

## 2 POLYMER SOLAR CELLS

This chapter gives an introduction to the relevant aspects of polymer solar cells.

### 2.1 Background

The active layer of PSCs usually consist of a blend of a conjugated polymer as light absorbing material and electron donor and a second material, often a fullerene derivative, as electron acceptor. To efficiently convert solar irradiation to electricity the conjugated polymer in a solar cell need to be able to absorb a substantial amount of the available photons. Which photon energies that can be absorbed are defined by the band gap ( $E_g$ ) and absorption coefficient of the semiconducting polymer. The absorption coefficient is described as the amount of photons a material absorbs at a given wavelength. Ideally, a material should absorb all available photons. For the potentially highest power output for a single layer cell the band gap should be between 1-1.5 eV or 1250-830 nm, as described by Shockley-Queisser (Figure 2.1). [9]

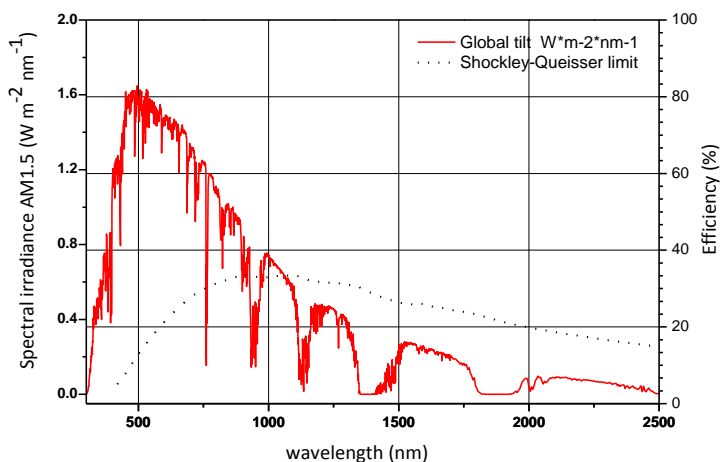
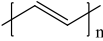
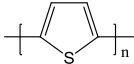
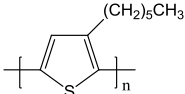
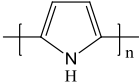
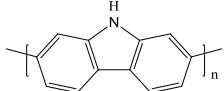


Figure 2.1: Standardized AM 1.5 solar irradiation spectrum (red) and Shockley-Queisser maximum efficiency limit for a single layer solar cell (black)

## 2.2 Conjugated polymers

The word polymer originates from the Greek words poly (many) and meros (parts). A polymer does indeed consist of many parts, called monomers, which are linked together in a long chain to form a polymer. Conjugated polymers consist of a backbone chain of alternating single and double bonds. Because of this there will be an overlap of p-orbitals which in turn enables delocalization of electrons across the polymer backbone, making it a one dimensional semiconductor. The semiconducting polymer comprises a highest occupied molecular orbital (HOMO) and a lowest unoccupied molecular orbital (LUMO). The band gap of the polymer is defined by the difference between these energy levels, which determines the minimum energy needed to excite an electron. The simplest example of a conjugated polymer is polyacetylene (Table 2.1), consisting of a single carbon chain with alternating single and double bonds. Conjugated polymers are promising for use as active material in e.g. solar cells, light emitting diodes and field-effect transistors. In order to produce commercial polymer electronics the polymers need to be solution processable and stable to ensure a long lifetime of the device. Due to the low conductivity and poor solubility of polyacetylene it is not suitable for solar cell applications. [10,11] Solubility is usually accomplished by incorporation of alkyl side chains. Solution processable polymers are necessary for low-cost device production through methods such as ink-jet printing or roll-to-roll processing. [12-14]

**Table 2.1:** Chemical structures of some conjugated polymers

Polymer	Chemical Structure
Polyacetylene	
Polythiophene	
Poly(3-hexyl thiophene), P3HT	
Polypyrrole	
Polyfluorene	
Polycarbazole	

Conjugated polymers based on aromatic units allows for easy chemical modification. This means that properties such as processability, opto-electronic properties and stability can be tuned by small changes in the polymers chemical structure, resulting in a library of polymers with a wide range of characteristics. Both the backbone and the side chains can be chemically modified to achieve different properties of the polymer, examples of this is alteration of the energy levels for a better coverage of the solar spectrum, or addition of alkyl side chains, which will influence both the solubility of the polymer and the interactions with acceptor molecules. In order to design polymers with high performance there is a need for a detailed understanding on how the chemical structure of the polymer influences the polymer properties and the performance of devices (Chapter 3).



Figure 2.2: Chemical structure of poly(paraphenylene); aromatic (left) and quinoid form (right)

For a polymer consisting of aromatic repeating units, the backbone has two resonance structures, i.e. the aromatic and the quinoid form (Figure 2.2). Due to the localized  $\pi$ -electrons the aromatic form is energetically more stable. However, when the  $\pi$ -electrons are delocalized single bonds are converted into double bonds and vice versa, making the polymer adopt the quinoid form. This form results in a more planar structure with reduced band gap and a red-shifted absorption. The lowest possible band gap is achieved when all bonds in the polymer are the same length, i.e. equal amount of aromatic and quinoid form. In order to stabilize the quinoid form, donor (D) and acceptor (A) units are co-polymerized to form a so called DA-structure. [15]

### 2.3 Fullerene derivatives

Today, the most utilized acceptors in PSCs are fullerene derivatives such as [6,6]-phenyl- $C_{61}$ butyric acid methyl ester (PC<sub>61</sub>BM) [16] or [6,6]-phenyl- $C_{71}$ butyric acid methyl ester (PC<sub>71</sub>BM) [17] (Figure 2.3). PCBM are preferred over fullerenes due to their solubility in organic solvents. This is a necessary property for solution processable donor/acceptor blends for “printable” solar cells.

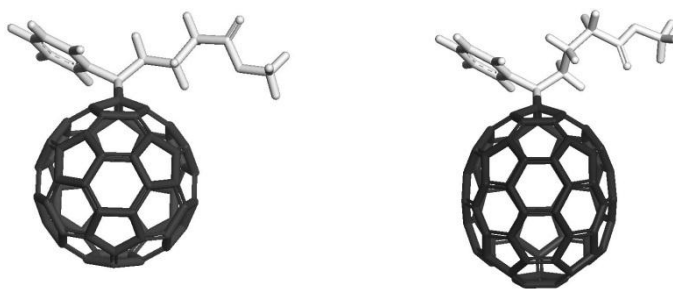


Figure 2.3: Chemical structures of (a) PC<sub>61</sub>BM and (b) PC<sub>71</sub>BM

Crystallization of the fullerenes will have a negative effect on the solar cell performance. Upon annealing the crystals can grow several micrometres, resulting in a poor morphology of the active layer. [18-20] The crystal growth can be limited by improving the thermal stability of the blend as will be further discussed in Chapter 5.

## 2.4 Device architecture

The earliest type of PSC was based on a single layer of polyacetylene and showed a very low efficiency. [21] The performance was later improved by the use of a bilayer structure. [22,23] Today, the most common device structure is the bulk-heterojunction (BHJ), in which the donor and acceptor components are intimately mixed in one layer (Figure 2.4). [24,25] This results in a large interfacial area between the donor and acceptor material which is beneficial for the formation of the charge-transfer state (CT-state) and charge separation (Section 2.5).

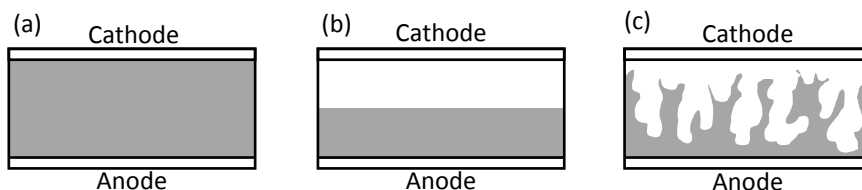


Figure 2.4: Schematics of different solar cell architectures; (a) single layer (b) bilayer and (c) BHJ

Lab-scale devices are usually prepared on glass substrates coated with indium tin oxide (ITO) as the anode. On top of the ITO, a thin layer of Poly(3,4-ethylenedioxythiophene)-poly(styrenesulfonate)) (PEDOT:PSS) is spin coated (Figure 2.5). This will lower the work function of the ITO and make the surface smoother. [26] The active layer with the polymer:fullerene blend is deposited on top of these layers, usually by spin coating. The cathode is then evaporated on top of the active layer. The cathode usually consists of an interlayer of e.g. lithium fluoride [27] followed by an aluminium layer. A schematic picture of two architectures is found in Figure 2.6.

## Polymer Solar Cells

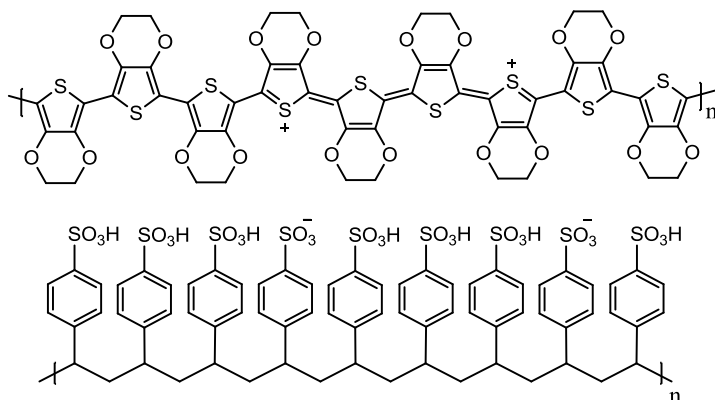


Figure 2.5: Chemical structure of PEDOT:PSS

PSCs are often divided into two types; conventional and inverted device architecture. In inverted polymer solar cells (iPSCs), ITO acts as the cathode instead of anode as in the conventional device architecture. The conventional (standard) architecture is the most common device structure for high performing PSCs. Unfortunately, the standard solar cells exhibit short operational life time caused by the oxygen- and water-sensitive cathode materials. The inverted device structure was developed to overcome this problem and has been shown to have a superior stability compared to standard solar cells. [28,29] On the contrary, inverted devices often show lower efficiency than conventional PSCs due to a too high work-function of the ITO cathode. To improve the electron collection efficiency (charge selectivity) at the cathode, and thereby the overall power conversion efficiency, significant effort has been made to modify the interface between the cathode and the organic photo-active layer. This will be further discussed in Chapter 4. Since inverted devices do not require a transparent bottom electrode other materials than ITO can be used as electrode material. [30-34] This is an advantage of inverted devices since ITO contains indium, which is both rare and expensive. [35] The use of more abundant electrode materials would therefore reduce the price of PSCs.

## Polymer Solar Cells

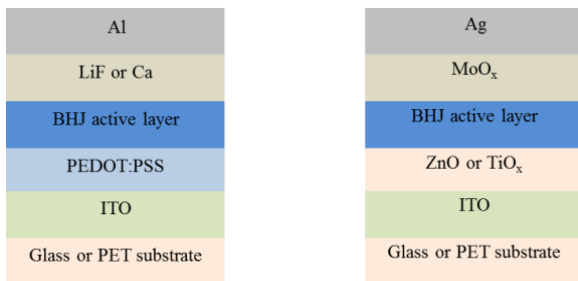


Figure 2.6: Schematic image of two different device architectures. Standard geometry (left) and inverted geometry (right)

### 2.5 Working principle of polymer solar cells

Figure 2.7 illustrates the working principle of solar cells. When the incident light reaches the active layer of a solar cell it is absorbed by the polymer if the energy of the photon is larger than the size of the polymer band gap. When a photon is absorbed it creates an exciton, i.e. a bound electron-hole pair, by exciting an electron from the HOMO to the LUMO of the polymer. The exciton then diffuses in the polymer-rich phase of the active layer until reaching a donor-acceptor interface. An exciton can diffuse approximately 5-8 nm before recombination occurs. [36-38] In PSCs employing the BHJ concept the large interfacial area makes it possible for the exciton to reach the donor-acceptor interface within this diffusion length. In a well-mixed blend, the donor and acceptor material are in direct contact with each other and therefore no diffusion is needed. At the donor-acceptor interface, electron transfer occurs and a CT-state consisting of an electron in the LUMO of the acceptor and a hole in the HOMO of the donor is formed. This is followed by charge separation of the CT-state into free charges and a subsequent charge transport to the electrodes where collection of charges occurs. Exciton dissociation can only take place if the LUMO of the donor and the LUMO of the acceptor are separated by  $\sim 0.3$  eV ( $\Delta\epsilon_s$ ) [39,40], otherwise it would not be energetically favourable for the electron to leave the donor and hence there would be no driving force for the electron transfer.

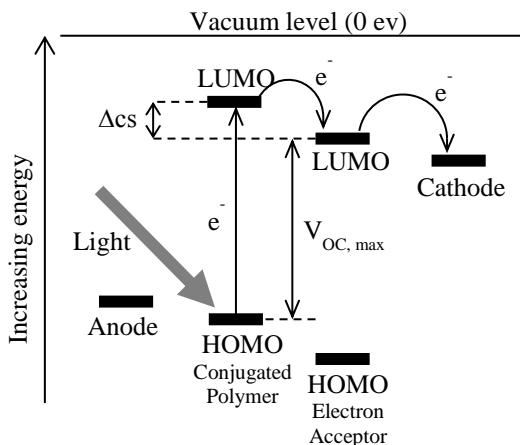


Figure 2.7: Working principle of a polymer solar cell

A good charge collection is important for the overall efficiency of a PSC. This means that the generated charges need to be transported to the electrodes without recombination. In order to achieve this, the active layer needs to offer continuous pathways for charge extraction. The challenge of generating both large interfacial area and continuous pathways to the electrodes simultaneously explains why it is important to be able to control the morphology of the active layer in order to produce PSCs with high efficiency. The morphology can partially be influenced by suitable choice of solvent or by addition of a small amount of slow evaporation solvent during spin coating. [41]

## 2.6 IV-characteristics

The performance of a PSC is usually evaluated by illumination of the device with a solar simulator. For northern European latitudes an air-mass (AM) 1.5G spectrum is used, corresponding to a solar inclination angle of  $48.2^\circ$ . The commonly used lamp intensity is called 1 sun ( $1000 \text{ W m}^{-2}$ ) and corresponds to the sunlight intensity on a bright day (no cloud coverage) at zero altitude on Earth.

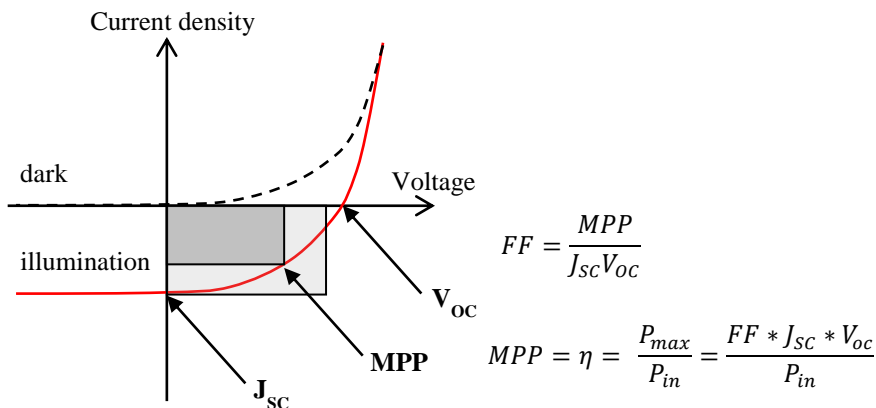


Figure 2.8: Current density-voltage characteristics for a solar cell

When illuminated, a PSC will generate a photocurrent. The devices are then evaluated using the IV-curve produced by normalising the generated photocurrent (I) in regard to device area and plotting it against the voltage (V) (Figure 2.8). Four important parameters extracted from the IV-curve are the short-circuit current density ( $J_{sc}$ ), which is the photocurrent divided by the area under short-circuit conditions, i.e. when no voltage is applied. The open-circuit voltage ( $V_{oc}$ ) is achieved at zero photocurrent. The  $V_{oc}$  of a device is dependent on the difference between the HOMO of the polymer and the LUMO of the acceptor and can be correlated to the energy of the CT-state. [42] The maximum power point (MPP) or solar cell efficiency ( $\eta$ ) is the point where the power is the highest. The fill factor (FF) describes the shape of the IV-curve and is given by the ratio between the MPP and the product of  $J_{sc}$  and  $V_{oc}$ .

## 2.7 Polymerization reactions

Over the years, many polymerization reactions have been used to synthesize conjugated polymers. [43] In the work presented in this thesis, Suzuki cross-coupling [44] and Stille cross-coupling [45] have been employed.

### 2.7.1 Suzuki cross-coupling polymerization

In 2010 Akira Suzuki, Ei-ichi Negishi and Richard F. Heck were awarded the Nobel Prize in chemistry for palladium-catalyzed cross couplings in organic synthesis. [46] The Suzuki cross-coupling reaction involves the formation of  $sp^2$ -hybridized carbon atoms. The method is described in Figure 2.9 and employs the use of a palladium catalyst and a base to facilitate the reaction between a halide or a triflate and a boronic compound. [44] The first step in the mechanism is oxidative addition of the halide to the palladium(0), forming a palladium(II) complex. The reaction cycle continues with a transmetalation step with the boronic compound, catalyzed by a base. In the final step, the product is expelled by reductive elimination, regenerating the palladium(0) catalyst.

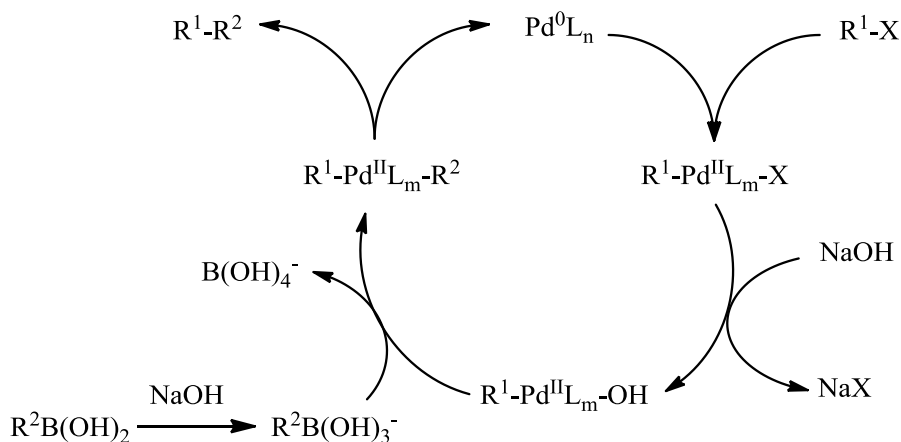


Figure 2.9: Reaction mechanism of a Suzuki cross-coupling reaction

### 2.7.2 Stille cross-coupling polymerization

The Stille cross-coupling reaction (Figure 2.10) involves the formation of  $sp^2$ -hybridized carbon atoms. The method employs the use of a palladium catalyst to facilitate the reaction between a halide or a triflate and an organotin compound. The reaction mechanism is similar to that of the Suzuki cross-coupling, the difference is the absence of a base in the Stille cross-coupling. This allows for polymerization of base sensitive monomers. A problem with the Stille reaction is the toxicity of the

organotin compounds. [47] This is a disadvantage compared to Suzuki cross-coupling, both at lab-scale and for future up-scaling of the process.

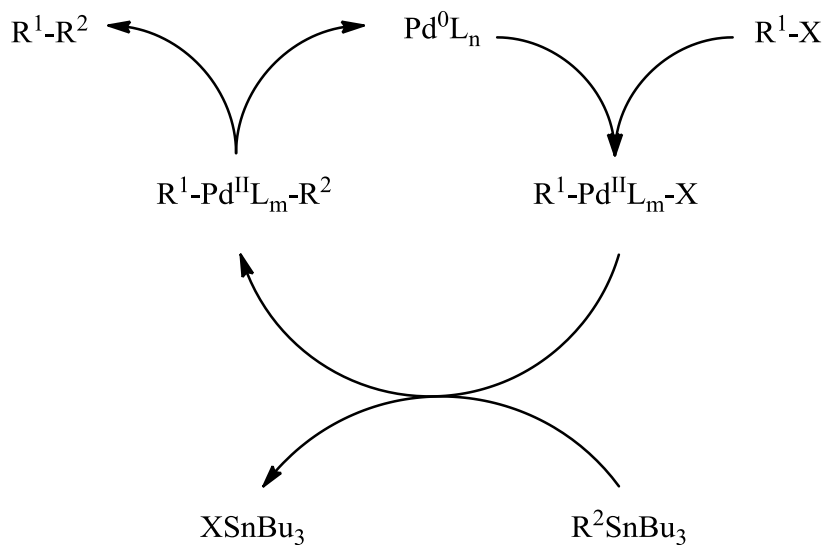


Figure 2.10: Reaction mechanism of a Stille cross-coupling reaction



## 3 DIKETOPYRROLOPYRROLE-BASED POLYMERS

---

In this chapter, a well performing polymer is modified with alkoxy side chains to investigate the effect of various polymer properties.

### 3.1 Introduction

The diketopyrrolopyrrole (DPP) unit (Figure 3.1) is an acceptor often used in conjugated polymers. It originates from a strongly colored dye commonly known as Ferrari Red, or Red Pigment 254. The synthesis of DPP can be performed in a few simple steps from commercial products, making it an attractive material for photovoltaic devices. Since DPP is a planar unit it promotes  $\pi$ - $\pi$  stacking, thereby promoting high charge carrier mobility. [48,49] The  $\pi$ - $\pi$  stacking and optical properties of the material can be tuned by adding different donor units to the DPP-copolymer backbone. [50,51] Attachment of alkyl side chains onto the nitrogen atoms in the DPP unit improves the solubility of the material, which is crucial for solution processability and film forming ability of the polymers. [52]

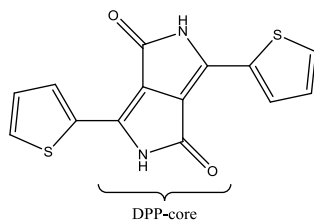


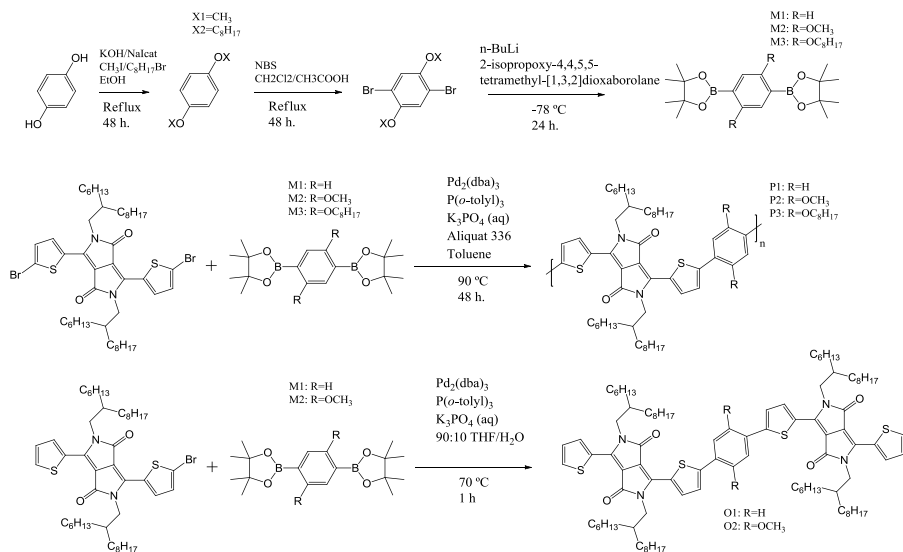
Figure 3.1: Chemical structure of the unsubstituted DPP unit used in this work

In 2010 Bijleveld et al. reported a copolymer based on 2,5-bis(2-hexyldecyl)-3,6-di(thiophen-2-yl)pyrrolo[3,4-c]pyrrole-1,4(2H,5H)-dione and a benzene spacer. Photovoltaic devices based on a blend of this copolymer (PDPPTPT, hereafter P1) and PC<sub>71</sub>BM reached good power conversion efficiency of 5.5% after optimization with a processing agent. [53] In an attempt to improve the properties of the polymer

alkoxy side chains were added on the phenyl spacer, resulting in a red shift in absorption. The oxygen gave rise to a shift of the HOMO level towards vacuum and thereby a reduced band gap. [54-57] However, structure-property relationships are usually not straightforward since a structural alteration usually affects additional properties aside from the desired ones which could have an impact on the final performance of a device. In an attempt to ascertain structure-property relationships more specifically derivatives of P1 was synthesized with methoxy (P2) and octyloxy (P3) side chains on the benzene ring. Also well-defined oligomers based on P1 and P2 were synthesized to verify structure-property relationships (Paper II).

### **3.2 Synthesis**

The benzene monomer was synthesized starting from hydroquinone. The dibrominated dialkoxy benzene was obtained after alkylation and subsequent bromination with NBS. The corresponding diboronate ester was attained after lithiation with n-butyllithium. The polymers were synthesized with Suzuki cross-coupling (Scheme 3.1). The monobrominated DPP-unit used for oligomer synthesis was attained after N-alkylation and bromination with NBS. The desired product was identified by matrix-assisted laser desorption/ionization time-of-flight (MALDI-TOF).



Scheme 3.1: Synthetic route for DPP-based polymers and oligomers

### 3.3 Physical and optical properties

The polymer synthesis resulted in reasonable molecular weights. The octyloxy side chains on P3 yielded a higher molecular weight due to improved solubility.

Table 3.1: Physical properties of polymers and oligomers

Material	M <sub>n</sub> (kg/mol) <sup>a</sup>	PDI	TGA <sup>b</sup> (°C)	T <sub>m</sub> <sup>c</sup> (°C)	T <sub>c</sub> <sup>c</sup> (°C)	HOMO <sup>d</sup> (eV)	LUMO <sup>d</sup> (eV)
<i>1% wt. loss</i>							
P1	15	1.5	415	>350	>350	-5.10	-3.58
P2	12	2.7	336	>300	260	-4.89	-3.55
P3	29	2.3	347	240	190	-4.88	-3.56
O1	-	-	257	153	110		
O2	-	-	341	181	148		

<sup>a</sup>Measured against polystyrene standard in TCB at 135°C, <sup>b</sup>under nitrogen atmosphere, 1% weight loss,

<sup>c</sup>determined from the 2<sup>nd</sup> heating scan via LUMO-E<sub>g, opt</sub> <sup>e</sup>calculated via oxidation or reduction peak onset, -(E<sub>red</sub> + 5.13)

Thermogravimetric analysis (TGA) (Table 3.1) indicated a good thermal stability but that it is somewhat decreased by introduction of the alkoxy side chains. Melting and crystallization temperatures were determined by differential scanning calorimetry (DSC) (Table 3.1). The results show a decrease of these temperatures with increasing length of the alkoxy side chain, caused by increased flexibility of the polymer chain. The opposite trend was observed for the oligomers, where the methoxy substituted oligomer (O2) display higher melting and crystallization temperature than the unsubstituted oligomer (O1). The cause of this result is unknown and needs to be further investigated. The difference in  $T_m/T_c$  trend between polymers and oligomers is likely caused by incomplete representation of the polymers by the oligomers due to symmetry reasons.

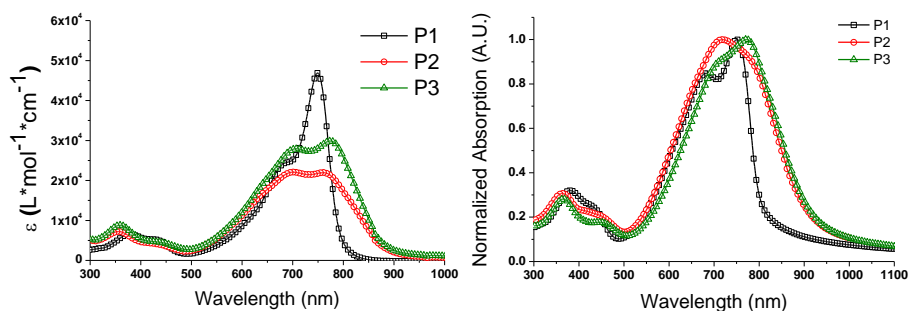


Figure 3.2: UV-Vis absorption of dilute polymer solutions ( $\text{CHCl}_3$ ,  $\sim 16 \text{ mg L}^{-1}$ ) (left) and solid state, spun from  $\sim 10 \text{ mg mL}^{-1} \text{ CHCl}_3$  solutions (right)

A redshift of absorption is seen for the alkoxy substituted polymers, both in chloroform solution and in thin film. This is caused by the shift of HOMO towards vacuum (Table 3.1) due to the electron donating effect of the alkoxy side chains. The alkoxy substituted polymers also show a broader and less strong absorption maxima in solution compared to P1, which has a higher solution absorption coefficient (Figure 3.2). This could be attributed to the stiffer backbone which either promotes intra chain aggregation or a more rod-like behavior which decreases the conformational distribution in the polymer chain, resulting in a less broad absorption. The increased flexibility of the alkoxy substituted polymer chains

compared to P1 indicated by these results will likely have an effect on the blend morphology and performance of the final PSCs.

### 3.4 Photovoltaic performance

Polymer:PC<sub>71</sub>BM solar cells were prepared using 1,8-diiodooctane (DIO) as co-solvent (Table 3.2). Both P2 and P3 based devices result in a lower voltage, likely caused by the reduced difference between the HOMO of the donor and the LUMO of the acceptor due to the electron donating effect of the alkoxy substitution. The lower current compared to P1 based devices is reflected in the lower external quantum efficiency (EQE) in the 600-800 nm absorption region (Figure 3.3).

*Table 3.2: Photovoltaic data of devices based on polymer:PC<sub>71</sub>BM blends*

Material	Polymer: PC <sub>71</sub> BM (w:w)	Thickness (nm)	RMS blend (nm)	J <sub>SC</sub> (mA/cm <sup>2</sup> )	V <sub>OC</sub> (V)	FF	η (%)
P1	1:2	125	2.77	8.4	0.78	49	3.2
P2	1:2	80	10.9	3.4	0.59	45	0.9
P3	1:2	77	4.27	7.1	0.60	46	2.0

Active layers spun from 5-15 mg mL<sup>-1</sup> polymer:CHCl<sub>3</sub> with 23 mg mL<sup>-1</sup> DIO. Device architecture ITO/PEDOT:PSS/active layer/Yb/Al

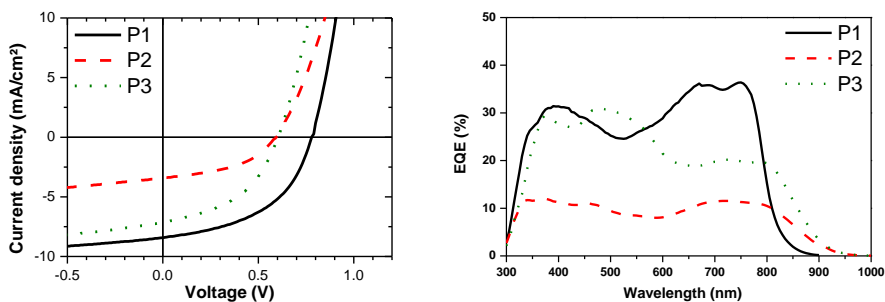


*Figure 3.3: IV-curve (left) and EQE (right) for Polymer:PC<sub>71</sub>BM solar cells*

P2 based devices show a drastically lower current compared to both P1 and P3 based devices. A possible explanation for this can be found via Atomic force microscopy (AFM), which reveals similar blend morphology for both the P1 and

P3:PC<sub>71</sub>BM based blends. Whereas the P2:PC<sub>71</sub>BM blend show a distinctly different morphology, which can be seen in Figure 3.4. However, here P1 display a lower photovoltaic performance then what has previously been reported. [53] It is therefore possible that both P2 and P3 might reach higher efficiencies after optimization with proper processing agents.

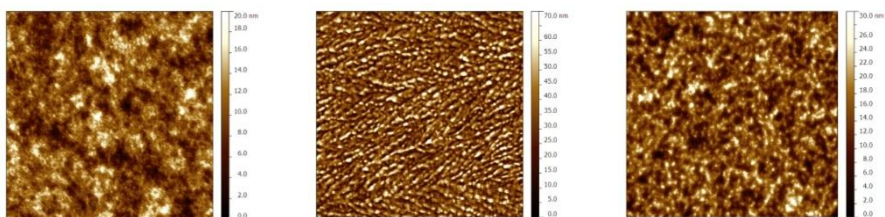


Figure 3.4: AFM topographical images (5x5  $\mu\text{m}$ ) for the P1, P2 and P3:PC<sub>71</sub>BM blends respectively

## 4 POLYMER INTERLAYERS

---

As discussed in Section 2.4 PSCs are often divided into two types; conventional and inverted device architecture. Problems found in inverted solar cells but not in standard devices must be related to device architecture. This Chapter describes the use of a conjugated polymer interlayer at the cathode to solve some of the problems related to the inverted device structure.

### 4.1 Introduction

Inverted polymer solar cells have shown a superior stability compared to devices with conventional architecture. However, losses are often found due to limitations at the active layer/electrode interface, which can reduce the device performance. Problems related to the device architecture of iPSCs are likely caused by electrical or surface properties of the electrodes. For example, iPSCs often show a lower PCE compared to conventional PSCs due to a too high work function of the ITO cathode. Both conventional and inverted solar cells are usually based on an ITO substrate. The work function of ITO is ~4.3-4.7 eV [58-61] which means that it is not aligned to either the HOMO of the donor or the LUMO of the acceptor. This non-ohmic contact at the ITO/donor and ITO/acceptor interface means that ITO is not a charge selective contact (i.e. can collect both electrons and holes) which will affect the maximum attainable  $V_{OC}$  of devices. To improve the charge selectivity of the cathode, and thereby the overall performance of the device, a lot of research has been put into modifying the interface between the cathode and the active layer. The requirements for an interlayer material is that it should provide a good ohmic contact with the acceptor material, efficiently transport electrons and block positive charges (hole blocking). In addition, the interlayer material should be stable and not increase the series resistance in the device. One way to improve the efficiency of iPSCs is by coating the cathode surface with a metal oxide layer, e.g. ZnO or TiO<sub>2</sub>. Unfortunately, the hydrophilic surface of the metal oxides can induce an undesired blend morphology of the active layer, thus having a negative effect on the solar cell performance. [62]

## Polymer Interlayers

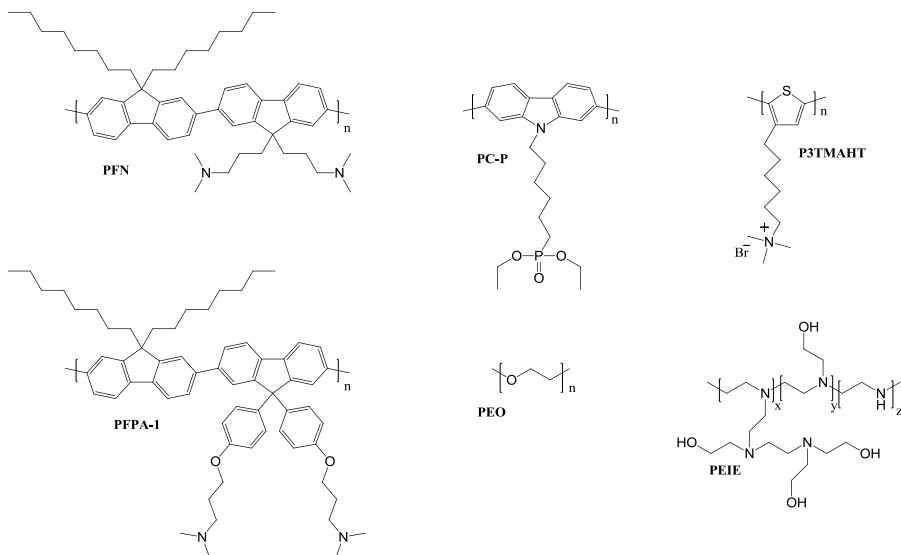


Figure 4.1: Chemical structures of some interlayer polymers used in organic photovoltaics

Conjugated polyelectrolytes and uncharged conjugated polymers (Figure 4.1) have been used as an alternative to the metal oxides to modify conditions for charge injection, energy level alignment and surface energy at the interface between the cathode and the active material in both light emitting diodes and PSCs. [63-66] The improvement in device performance arises from changes in electronic and orbital interactions at the interface. The interlayer material is chemically or physically absorbed onto the electrode surface, creating a molecular dipole at the surface. It has been shown that polymer interlayers can induce a shift in the work function of not only ITO but also other cathode materials, such as metals, metal oxides and graphene. [66,67] The altered work function of the cathode is a better match to the LUMO level of the acceptor in the active layer, resulting in an improved electron extraction. The solution processability and mechanical robustness of the polymer interlayers make them a good alternative to metal oxides.

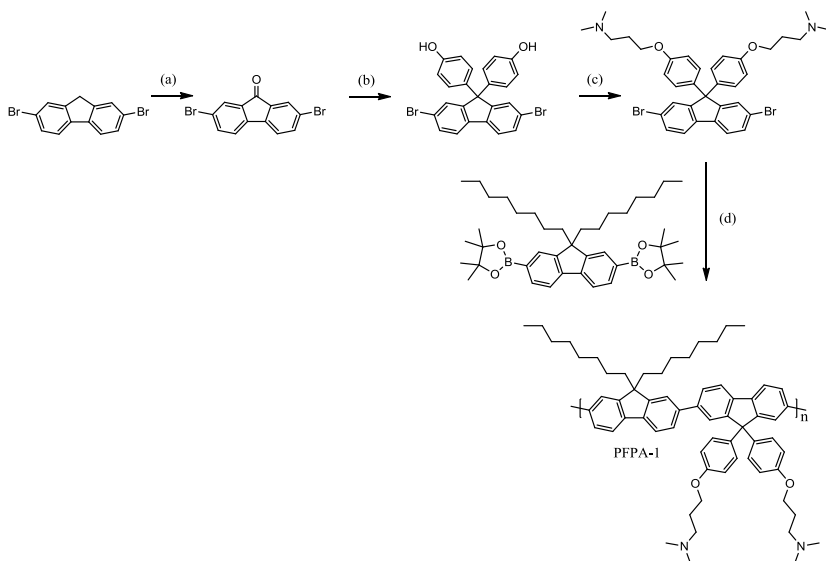
## 4.2 ITO free inverted polymer solar cells

Today, most organic solar cells are constructed on ITO covered substrates, which considerably increases the production cost of PSCs. It would therefore be very beneficial to replace the ITO with a less expensive electrode material. Consequently, inverted ITO-free solar cells (iFSCs) was introduced, based on an Al cathode coated with a layer of Ti or Cr to prevent formation of aluminium oxide at the cathode surface. However, this type of solar cell architecture has not attracted much attention due to the low photovoltaic performance compared to solar cells with more conventional device structures. The problem with low performance is related to the device architecture and is likely caused by the electrical properties of the electrodes or surface properties of the cathode. In Paper I, an ultrathin cathode interlayer of an uncharged conjugated polymer, poly(3,3'-([(9',9'-dioctyl-9H,9'H-[2,2'-bifluorene]-9,9-diyl)bis(4,1-phenylene)]bis(oxy))bis(N,N-dimethylpropan-1-amine)) (PFPA-1), is used to overcome some of the electrical and morphological issues with iFSCs. PFPA-1 was designed to be a hole blocking layer with a deep lying HOMO level and a wide band gap, thereby increasing the charge selectivity and in turn FF due to a reduction in surface recombination of holes at the cathode interface. The amine groups at the end of the side chains will induce a dipole, thus enabling the polymer to bind to the cathode surface, thereby influencing the work function of the cathode. The change in work function is proportional to the magnitude of the dipole and is therefore sensitive to the alignment of polar and non-polar groups relative to the substrate.

### 4.2.1 Synthesis

The synthetic route and reaction conditions for PFPA-1 are depicted in Scheme 4.1. Starting from 2,7-dibromofluorene, 2,7-dibromo-9H-fluoren-9-one was obtained after oxidation. [68] The product was then reacted with phenol according to literature procedures. [69] The amine-substituted monomer was thereafter accessed via an alkylation reaction with 3-dimethylamino-propylchloride hydrochloride and purified by column chromatography. The polymerization between the amine-

substituted monomer and the boronic ester was performed with Suzuki cross-coupling.



Scheme 4.1: Synthetic steps to PFPA-1. Reaction conditions: (a)  $\text{CrO}_3$ ,  $\text{Ac}_2\text{O}$ ; (b) Phenol, MSA,  $\text{HS}(\text{CH}_2)_2\text{COOH}$ ; (c)  $\text{K}_2\text{CO}_3$ ,  $\text{Cl}(\text{CH}_2)_3\text{N}(\text{CH}_3)_2$ ; (d)  $2\text{Pd}^0(\text{dba})_3$ , Aliquat 336,  $\text{K}_3\text{PO}_4$ , Tri-*o*-tolylphosphine

#### 4.2.2 Energy levels

Square-wave voltammetry (SWV) measurements (Figure 4.2) show the HOMO and LUMO levels of PFPA-1 to be 6.1 eV and 2.9 eV. The deeper lying HOMO, compared to TQ1 in the active layer (5.7 eV) [70], could reduce the undesired charge flow at the cathode interface, thus leading to an improved FF.

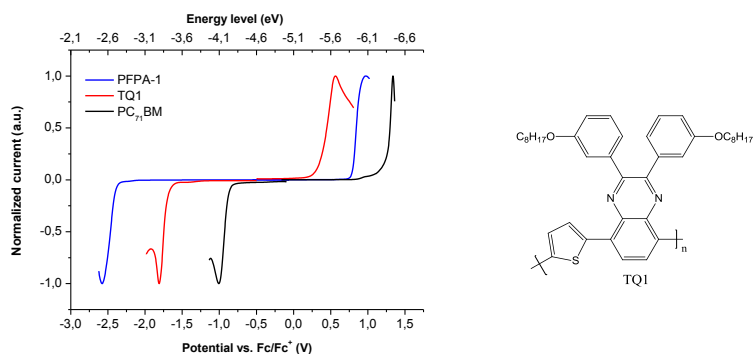


Figure 4.2: SWV of the thin films of PFPA-1, TQ1 and PC<sub>71</sub>BM (left) and chemical structure of TQ1 (right)

### 4.2.3 Photovoltaic performance

Conventional and iFSCs were constructed using PC<sub>71</sub>BM as acceptor according to the device structures in Figure 4.3. PFPA-1 was spin coated on top of the TiO<sub>x</sub> surface from toluene solution and then rinsed with neat toluene or o-dichlorobenzene solvent to remove most of the physically absorbed polymer, leaving an ultrathin (<10 nm) layer of PFPA-1.

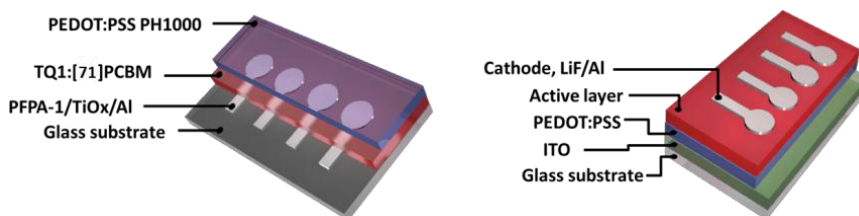


Figure 4.3: Schematic device structure of iFSC (left) and conventional solar cell (right)

Performance parameters are listed in Table 4.1. The iFSC incorporating the PFPA-1 interlayer show considerably higher FF than the solar cells with the unmodified cathode. The increase in FF is ascribed to the hole blocking ability of the interlayer, resulting in a reduced undesired charge flow at the cathode interface. The increased

FF is also seen in the IV-curves where the iIFSCs with PFPA-1 show a reduction in the dark current (Figure 4.4).

**Table 4.1:** Photovoltaic performance of solar cells based on TQ1:PC<sub>71</sub>BM

Device architecture	J <sub>sc</sub> (mA/cm <sup>2</sup> )	V <sub>oc</sub> (V)	FF	η (%)
Conventional	8.98	0.87	0.67	5.23
Inverted without PFPA-1	8.82	0.78	0.53	3.65
Inverted with PFPA-1	10.40	0.78	0.64	5.19

Devices with PFPA-1 also show an increase in J<sub>sc</sub> compared to both conventional devices and iIFSCs without PFPA-1. The reason for this is most likely an effect of increased surface area between donor and acceptor due to a more beneficial morphology caused by a change in the cathode surface energy. [62,71]

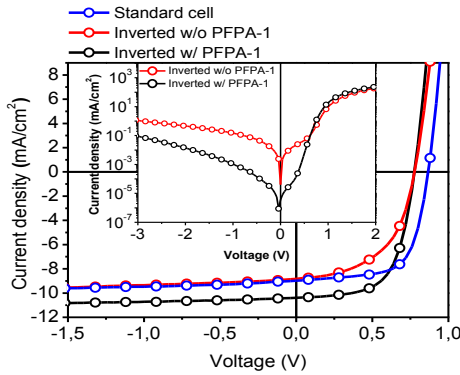


Figure 4.4: IV-curves for the solar cells under illumination. Inset: Dark IV-curves for the iIFSC with and without PFPA-1

#### 4.2.4 Surface modification

The surface energy of the TiO<sub>x</sub>/Al cathode was investigated with water contact angle measurements on both PFPA-1 modified and unmodified electrode. It is clear that there is a major change in surface energy (Figure 4.5). The neat metal surface showed a highly hydrophilic surface with a contact angle of 13° whereas the PFPA-1 treated surface had a contact angle of 70°. This clearly shows that there is still

PFPA-1 on the cathode surface after rinsing with neat solvent that will not be redissolved into organic solvents. The free electron pair on the PFPA-1 side chains likely binds to acidic sites on the  $\text{TiO}_x$  surface. It has previously been shown that acidic surface sites of  $\text{TiO}_2$  coordinate to pyridine end groups in dyes, relevant for Grätzel solar cells. [72]

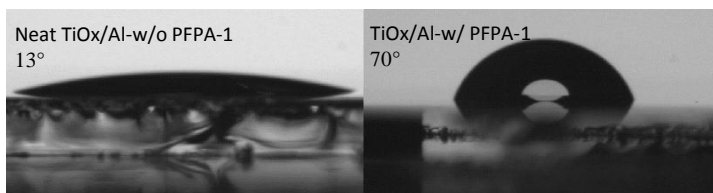


Figure 4.5: Water contact angle of neat  $\text{TiO}_x$  without PFPA-1 (left) and with PFPA-1 (right)

A difference in morphology between PFPA-1 modified and unmodified sample is observed with topographical AFM images. This difference could correspond to a finer structure with increased interfacial area between donor and acceptor, resulting in the significant increase in  $J_{\text{SC}}$  for devices with PFPA-1 (Figure 4.6). In untreated samples, there is a stronger phase separation between TQ1 and  $\text{PC}_{71}\text{BM}$  and the root mean square (RMS) surface roughness is 1.37 nm. In the PFPA-1 treated samples the active layer is more homogenous with an RMS value of 0.862 and a visibly more even surface.

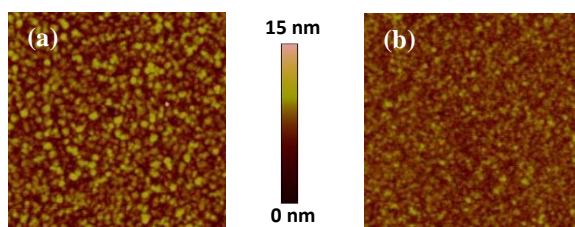


Figure 4.6: AFM topography images ( $2\ \mu\text{m} \times 2\ \mu\text{m}$ ). (a)  $\text{TQ1}:\text{PC}_{71}\text{BM} = 2:5$  on  $\text{TiO}_x/\text{Al}$  (RMS = 1.37 nm), (b)  $\text{TQ1}:\text{PC}_{71}\text{BM} = 2:5$  on PFPA-1 modified  $\text{TiO}_x/\text{Al}$  (RMS = 0.862 nm)

### **4.3 Influence on device stability**

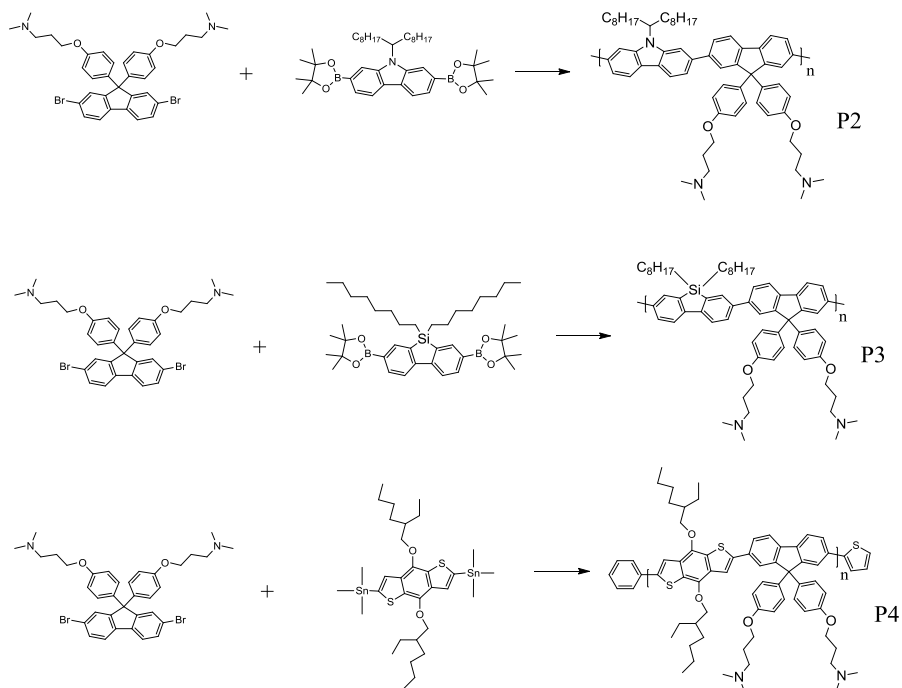
Inverted polymer solar cells often show an improved long-term stability compared to conventional PSCs. [73,74] Even though the use of an interlayer is necessary to improve the photovoltaic performance of inverted devices, not much work has been done on how the chemical structure of these interlayers and their stability influence the life time of the final device. In Paper III, the structure-property relationship in respect to stability of four polymer interlayer materials is evaluated on both device performance and stability. The results are compared to both devices using TiO<sub>2</sub> [75] as interlayer as well as devices with no interlayer. The well-studied conjugated polymer P3HT is used in the active layer together with PC<sub>61</sub>BM.

#### **4.3.1 Synthesis**

The chemical structures of monomers and polymers P2-P4 are shown in Scheme 4.2. PFPA-1 is here called P1 and used as reference to previous work as it has shown excellent performance as interlayer material in iPSCs. The three new interlayer materials are partially derived from PFPA-1 but the fluorene monomer has been exchanged to carbazole (P2), silafluorene (P3) and benzodithiophene (P4) units respectively. These structures have previously been reported to have a higher photochemical stability than fluorene. [76,77]

Polymers P1-P3 was synthesized with Suzuki cross-coupling. P4 was synthesized with Stille cross-coupling and then end capped with 2-(tributylstannyl)-thiophene and bromobenzene subsequently to remove the residual stannyl end groups.

## Polymer Interlayers



Scheme 4.2: Chemical structures of monomers and polymers (P2-P4)

### 4.3.2 Energy levels

As seen in Figure 4.7, all the interlayer materials have a deeper lying HOMO level (between -5.7 eV and -6.1 eV) than P3HT (-5.3 eV) and the ITO cathode (~ -4.3 eV). As a result of this, all four interlayers have hole-blocking abilities and can thus contribute to an improved FF in iPSCs. The benzodithiophene unit will act as a stronger donor than the other monomers, resulting in a smaller band gap in P4 compared to the other three interlayer polymers. Both the HOMO and the LUMO level are closer to the energy levels of P3HT than in the other three polymers, which have similar HOMO and LUMO levels.

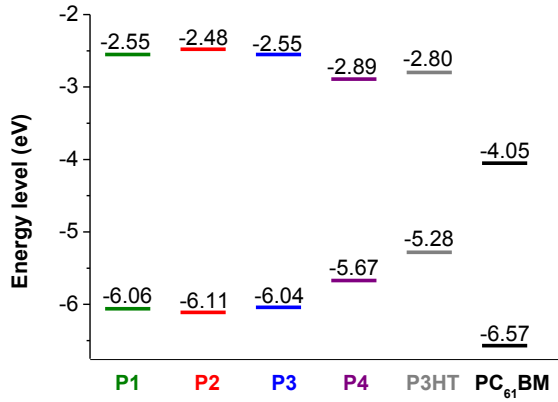


Figure 4.7: Energy level diagram for the four interlayer polymers (P1-P4) as well as for the materials in the active layer (P3HT and PC<sub>61</sub>BM)

### 4.3.3 Polymer stability

To investigate the photo-chemical stability of the interlayers, thin polymer films were spin-coated on glass. The samples were illuminated under 0.5 sun intensity with a solar simulation system in ambient air. During illumination, the samples were placed on a black metal surface holding 50 °C. The UV-Vis absorbance spectra of the samples were recorded from 300 to 1100 nm. The degradation of the polymers was monitored by the maximum peak value. The remaining peak absorbance ( $A_{max, remaining}$ ) relative to the start value of the peak absorbance ( $A_{max, start}$ ) was used to monitor the degradation:

$$A_{max,remaining} = \frac{A_{max}}{A_{max,start}} \times 100$$

where  $A_{max}$  is the maximum absorbance at given point.

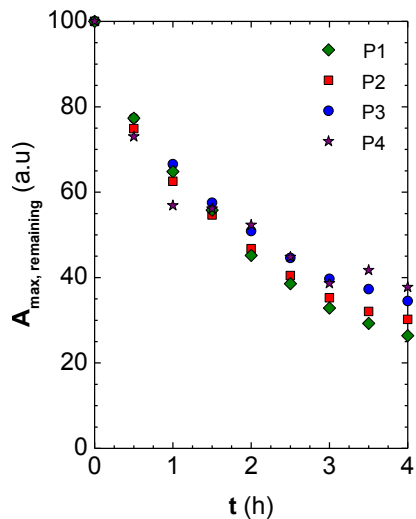


Figure 4.8:  $A_{\max, \text{remaining}}$  measured with a UV-Vis spectrometer on thin films of P1 (diamonds), P2 (squares), P3 (circles) and P4 (stars) after aging under simulated solar irradiation

As seen in Figure 4.8, the four interlayer polymers have similar photo-chemical stability but P1 possess a slightly higher degradation rate ( $A_{\max, \text{remaining}} \sim 25\%$  after 4h) compared to P3 ( $A_{\max, \text{remaining}} \sim 35\%$  after 4h) which seem to be somewhat more stable. It seems like the stability of the polymer interlayers are mainly affected by incorporation of the amine-containing moiety since this unit is present in all four polymers.

#### 4.3.4 Photovoltaic performance and life time

Device stability was measured on non-encapsulated samples following the ISOS-L-2 protocol. [78] Samples were exposed to continuous illumination of 1 sun intensity and AM1.5G spectrum filter in N<sub>2</sub> atmosphere. The initial performance of P1, P3 and P4 is 3.12 % compared to 3.6 % of a sample using TiO<sub>2</sub> as interlayer. The initial and final (after 400 h ageing) device parameters are listed in Table 4.2. All the interlayers improve the device performance significantly compared to devices without interlayer. The major effect of the interlayers is the stabilization of the V<sub>OC</sub> where both the polymer interlayers and the TiO<sub>2</sub> reduce the degradation of the V<sub>OC</sub> in the so called burn-in stage during the first 100 h (Figure 4.9). The drop in V<sub>OC</sub> and FF for devices without interlayer is likely caused by the shift in work function of the ITO cathode when illuminated with UV-light, leading to a non-ohmic contact at the interface between the electrode and the active layer. [79] The reduction of J<sub>SC</sub> is slightly higher in devices with polymer interlayers than in devices with TiO<sub>2</sub>. However, it is difficult to determine the effect of the interlayers as the drop in J<sub>SC</sub> is strongly influenced by structural changes in the P3HT:PC<sub>61</sub>BM blend. [80]

**Table 4.2:** Device performance initially and after 400 h of ageing, the reference sample is without any interlayer. Values are averaged over 8-12 cells on the same substrate measured on devices with inverted architecture and the following stack: ITO/interlayer/P3HT:PC<sub>61</sub>BM/MoO<sub>3</sub>/Ag

Interlayer	Initial				After 400 h			
	V <sub>OC</sub> (V)	J <sub>SC</sub> (mA/cm <sup>2</sup> )	FF	PCE (%)	V <sub>OC</sub> (V)	J <sub>SC</sub> (mA/cm <sup>2</sup> )	FF	PCE (%)
Reference	0.53	8.37	49.66	2.18	0.44	5.99	47.19	1.23
P1	0.60	8.59	61.52	3.12	0.59	5.91	59.94	2.06
P2	0.59	8.60	55.07	2.78	0.56	6.23	57.35	2.05
P3	0.60	8.56	61.74	3.12	0.59	5.57	56.63	1.82
P4	0.60	8.54	61.06	3.12	0.58	6.23	63.72	2.27
TiO <sub>2</sub>	0.60	8.62	69.30	3.60	0.58	7.41	58.42	2.51

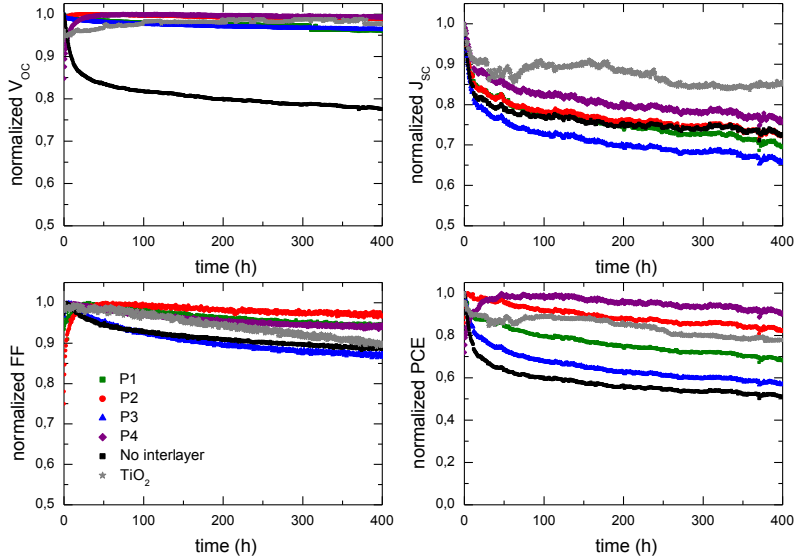


Figure 4.9: Evolution of the device performance under continuous solar illumination of inverted cells with different interlayers. Values are averages on 2-4 cells and normalized to their initial level. Samples are kept at  $40 \pm 5$  °C

The information from the device performance and ageing together with the photochemical stability of the polymers can allow for selection of the interlayer material with the most robust performance. In this particular study, that material seems to be P4, although the differences between the long-term stabilities are small. In general, there are no major differences, neither between the different polymer interlayers, nor between the polymers and  $TiO_2$ . However, processing of  $TiO_2$  has been extensively optimized for high initial performance and stability, which was not the case for the polymer interlayers. In oxide layers the interstitial states and variation in oxygen content can lead to significant variation in performance and stability. [81] Due to lack of such structural variability, polymer interlayers can offer a more reproducible process.

### 4.3.5 Electrode stability

In Paper V, PFPA-1 and PEIE (Figure 4.1) are used to modify ITO electrode surfaces in order to investigate the resultant work function and its stability in ambient atmosphere. Concordant with previous studies, Ultraviolet photoelectron spectroscopy (UPS) measurements of PEIE and PFPA-1 covered ITO was found to reduce the work function from 4.6 eV to 3.5 eV and 3.65 eV respectively. [66,82] After the initial work function measurements the samples were exposed to air and moisture by on-shelf storage at room conditions. Subsequent UPS measurements were performed on the samples 24 hours, two weeks and four weeks after the first measurement (Figure 4.10). After 24 hours of air exposure the work function for PEIE modified ITO was unchanged, whereas PFPA-1 modified ITO had an increased work function of 3.8 eV hence indicating that PEIE modified ITO samples are slightly more stable in the first 24 hours. After ageing for two weeks the work function of PEIE modified ITO was measured to 3.8 eV and the work function of PFPA-1 modified ITO had increased to 4.1 eV. The work function of the samples was found to stabilize in two weeks thus the work function was unchanged after 4 weeks of ageing.

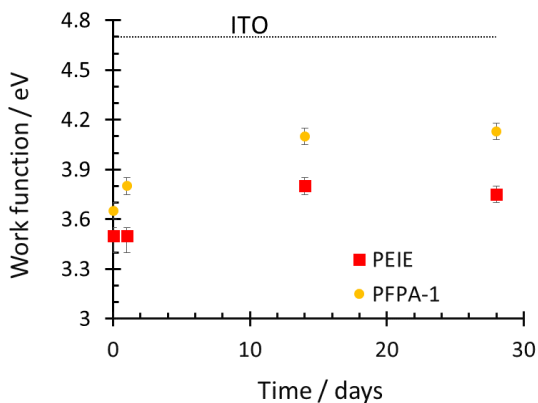


Figure 4.10: Change in work function of PEIE and PFPA-1 modified ITO measured over a period of 4 weeks

To understand the origin of the change in work function, metastable induced electron spectroscopy (MIES) [82] was used to study PEIE and PFPA-1 modified

ITO samples and changes induced as a function of time. MIES is a highly surface sensitive technique which measures the electronic density of only the topmost surface and is therefore sensitive to molecular orientations, whereas UPS has a probing depth of  $\sim 2\text{-}3$  nm. The MIES data are displayed in Figure 4.11 (a) and (b). The intensity of the peak at 4 eV that corresponds to the N-side groups and OH groups was reduced to  $\sim 80\%$  after two weeks for the PEIE modified ITO. This suggests a rearrangement of the OH and N-side groups away from the surface, changing the composition of the surface and thereby resulting in an increase in work function.

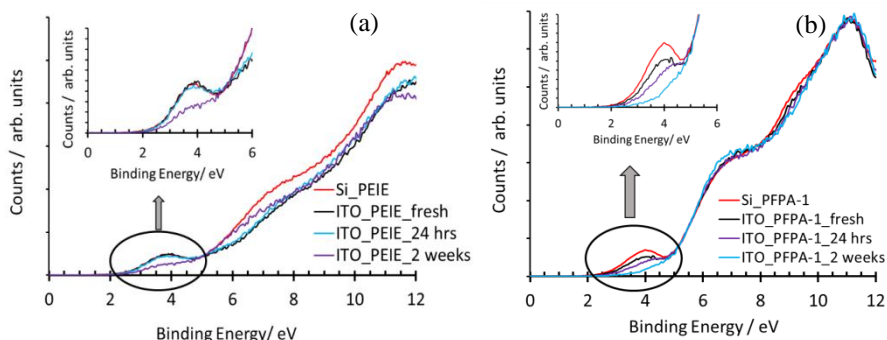


Figure 4.11: MIES spectra of (a) PEIE and (b) PFPA-1 films on Si and ITO

For the PFPA-1 modified ITO the peak at 4 eV practically disappears after two weeks thus suggesting a complete re-orientation of the polar side chains towards the substrate, resulting in an aliphatic carbon dominated surface. However, after two weeks of ageing in ambient air atmosphere the work function of PEIE and PFPA-1 modified ITO was still 0.8 eV and 0.5 eV lower than for unmodified ITO and comparable to the work function of Al, Ag and ZnO [83] that are commonly used as cathode or cathode interfacial layers in organic solar cells. The work function of these modified electrodes can therefore be regarded as fairly stable under ambient conditions and potentially suitable for use in roll-to-roll production.

## Polymer Interlayers

## 5 FULLERENE DERIVATIVES

---

In this chapter, two fullerene derivatives are used to simultaneously achieve both work function modification of the electrode and improved thermal stability of inverted polymer solar cells.

### 5.1 Introduction

As mentioned in Chapter 2, the active layer of a polymer solar cell consists of a fine blend of a donor polymer and an electron accepting fullerene derivative. The blend nanostructure is critical for achieving a high photovoltaic performance. The use of roll-to-roll processing for large scale production is one advantage of polymer solar cells. However, several issues must be resolved before the efficiencies of lab-scale devices can be reproduced. Two critical aspects concern (1) the inverted geometry of large-area devices that typically require modification of the bottom electrode with interlayers, and (2) the thermal stability of the polymer:fullerene bulk-heterojunction nanostructure. Unfortunately, suitable interlayer materials tend to be unstable under ambient conditions, which is a prerequisite for a large scale roll-to-roll production process. A self-assembly approach can be employed to circumvent the poor air stability of interlayer materials, as for instance demonstrated by Ma et al. [84] A second fullerene derivative that featured a tertiary amine-functionalized tail was added to a poly(3-hexylthiophene):fullerene blend. Self-assembly of the functionalized fullerene on the bottom electrode during spin-coating led to the formation of an interlayer that favorably modified the surface energy of the electrode hence reducing the driving force for vertical phase separation of the photovoltaic blend. The incorporation of a self-assembling cathode interlayer directly into the active layer blend is beneficial for roll-to-roll processing techniques as it removes the step of fabricating an additional layer of interface material before deposition of the active layer.

The roll-to-roll process usually involves several heating steps in order to achieve rapid solvent removal. Polyethylene terephthalate (PET) is the most likely substrate

and permits processing temperatures of up to 140 °C. [77,85] It is therefore crucial that the polymer:fullerene blend nanostructure is thermally stable at these conditions. The non-equilibrium nanostructure that the polymer:fullerene blends tend to form after deposition from solution can usually be preserved as long as the material is kept below the blend glass transition temperature [20,86,87], which for most materials is lower than the required processing and operating temperatures. When heated above this temperature, polymer:fullerene blends tend to coarsen and in addition, micrometer sized fullerene crystals start to grow [88,89], which is detrimental for the device performance as they act as charge traps and inhibit efficient charge transport to the electrodes. [18-20] The thermal stability of the blend can be improved by using different fullerene mixtures or nucleation agents that will either hinder the crystallization [90-94] of the fullerene or result in a controlled nucleation, reducing the crystal size. [95,96] Depending on the functionalization of the second fullerene, it can also be used as a self-assembling interlayer. [84] This will provide a more favorable surface energy of the electrode, thereby reducing the driving force for vertical phase separation of the polymer:fullerene blend.

In paper IV the effect of incorporating two different fullerene derivatives (PCBA and PCBP, Scheme 5.1) into the active layer of inverted TQ1:PC<sub>61</sub>BM solar cells were investigated in regard to the blend nanostructure, thermal stability and device performance. The chemical structures of the fullerene derivatives (Figure 5.1) in paper IV was designed in such a way as to provide good characteristics for modification of the cathode interface together with the supposition of positive effects on the blend nanostructure and thermal stability. The amine group on PCBA is similar to the one on the polymers described in Chapter 4. This type of amine group has previously been shown to adsorb to a number of different substrates, including ITO [97], and is therefore likely to induce an enrichment of PCBA at the cathode. The nitrogen atom in the pyridine group on PCBP has similar chemical properties as the tertiary amine on PCBA and is therefore also expected to enrich at the ITO cathode. In addition, pyridine groups, have been reported to coordinate to

C<sub>60</sub> [98], thus providing a prospect for a more thermally stable device and blend nanostructure [99].

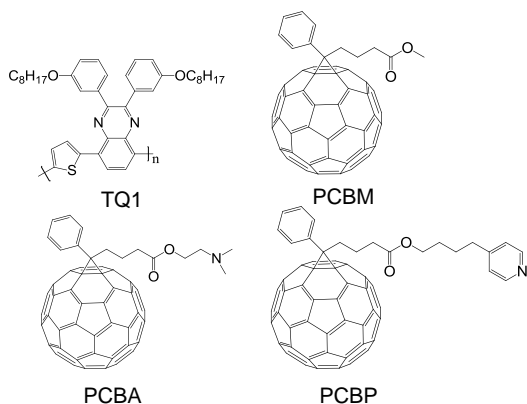
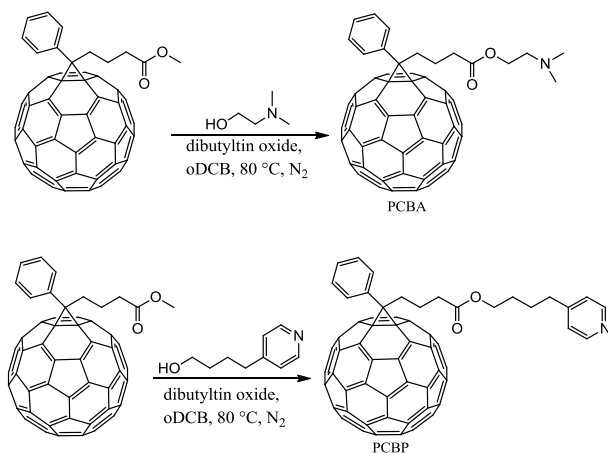


Figure 5.1 Chemical structures of TQ1, PCBM, PCBA and PCBP

## 5.2 Synthesis

PCBA and PCBP were synthesized starting from PC<sub>61</sub>BM using a simple transesterification reaction. PCBM and 2-(dimethylamino)ethanol (for PCBA) or 4-(pyridin-4-yl)butan-1-ol (for PCBP) are dissolved in ortho-dichlorobenzene (oDCB) in a 1:10 molar ratio. A 0.4 molar equivalent of dibutyltin oxide is added as catalyst. The mixture is heated to 80 °C under N<sub>2</sub> atmosphere and monitored by MALDI-TOF until completion. The resulting mixture is precipitated into MeOH and filtered. The obtained dark brown powder is subsequently purified with a short silica column (9:1 CHCl<sub>3</sub>:MeOH) to remove the remaining catalyst. The product was then precipitated into MeOH, filtered and dried.

Yield: PCBA 16 % (166 mg, 0.17 mmol), PCBP 88 % (1 g, 0.97 mmol). The yield for PCBA was significantly lower due to large amounts of side reactions occurring during the synthesis.



Scheme 5.1: Synthetic route for PCBA (top) and PCBP (bottom)

### 5.3 Surface modification

During deposition of the active layer, the amine-functionalized fullerene derivative tends to self-assemble at the interface of the ITO cathode. This self-organization is driven by differences in surface energy of the blend components and modifies the surface energy of the ITO electrode. UPS measurements were conducted to investigate the fullerenes' influence on the work function of ITO. The ITO work function was measured to 4.7 eV while both PCBA and PCBP modified ITO exhibited a reduced work function of 3.8 eV, thus showing that both fullerene derivatives can be used to alter the surface work function of ITO. The change in substrate surface energy was concluded by measuring the water contact angle on ITO-substrates. Thin films of TQ1:PCBM:PCBA and TQ1:PCBM:PCBP ternary blends and reference TQ1:PCBM were spin-coated onto ITO substrates. The samples were then rinsed with neat oDCB to remove non-chemisorbed material. The contact angle for cleaned ITO was  $\sim 20^\circ$  and  $58^\circ$  after treatment with oDCB. ITO samples with reference TQ1:PCBM or ternary blend displayed an initial contact angle of  $\sim 95^\circ$  (Table 5.1). After washing with oDCB there is a clear difference in contact angle for these surfaces which is ascribed to chemisorption of

PCBA or PCBP onto the ITO. This implies that a layer of PCBA or PCBP is present at the ITO surface in the ternary blends.

*Table 5.1: Water contact angle measurements*

Sample	Contact angle (°)	Contact angle after washing with oDCB (°)
ITO	~20	58
ITO/TQ1:PCBM 1:1	95	50
ITO/TQ1:PCBM:PCBA 1:0.8:0.2	94	88
ITO/TQ1:PCBM:PCBP 1:0.8:0.2	96	84

### 5.3 Blend nanostructure and thermal stability

The crystallization of PCBM was examined by optical microscopy (Figure 5.2). Solutions of 1:1 TQ1:PCBM, 1:0.9:0.1 TQ1:PCBM:PCBA and 1:0.9:0.1 TQ1:PCBM:PCBP were spin coated from (oDCB, 25 g L<sup>-1</sup>) and annealed at 140 °C for 15 min. Large micrometer sized crystals are clearly visible in the annealed TQ1:PCBM film (Figure 5.2 b), whereas no visible crystals are found in the films incorporating PCBA or PCBP (Figure 5.2 c, d).

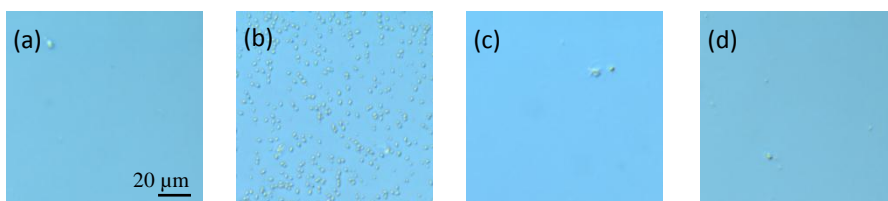


*Figure 5.2: Optical micrographs of (a) 1:1 TQ1:PCBM as cast, (b) 1:1 TQ1:PCBM, annealed 140 °C, 15 min, (c) 1:0.9:0.1 TQ1:PCBM:PCBA, annealed 140 °C, 15 min and (d) 1:0.9:0.1 TQ1:PCBM:PCBP, annealed 140 °C, 15 min*

Scanning electron microscopy (SEM) of annealed films also feature micrometre sized PCBM crystals and in addition a coarser nanostructure for neat TQ1:PCBM compared to e.g. TQ1:PCBM:PCBA (Figure 5.3). This is also seen by AFM measurements of 1:1 TQ1:PCBM, 1:0.8:0.2 TQ1:PCBM:PCBA and 1:0.8:0.2 TQ1:PCBM:PCBP films before and after annealing as evidenced by an increase in surface roughness  $R_{\text{rms}}$  from 0.5 nm to 1.8 nm for the reference sample (measured in between the crystals). Instead, annealed ternary blend films continue to display a

low  $R_{\text{rms}}$  of 0.5-0.6 nm. Furthermore, the difference in blend nanostructure is confirmed by photoluminescence (PL) spectroscopy (Figure 5.4) where the neat TQ1:PCBM film show a much higher PL intensity after annealing compared to the films incorporating PCBA and PCBP. This suggests a finer intermixed blend for the samples with PCBA and PCBP with better contact between the polymer and fullerene molecules.

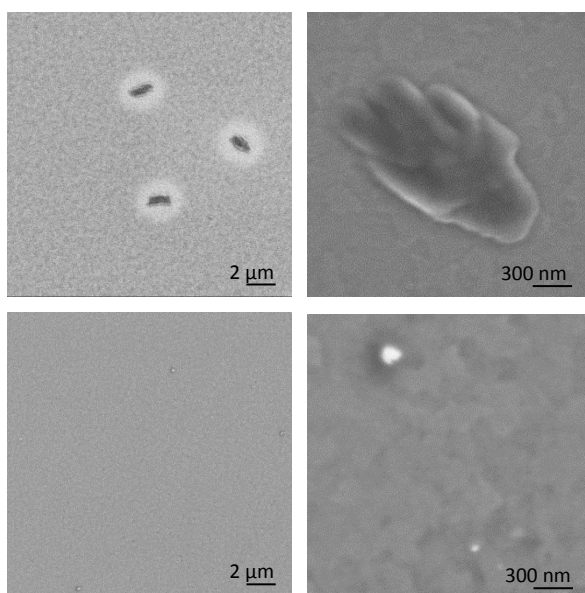


Figure 5.3: SEM micrographs of 1:1 TQ1:PCBM (top) and 1:0.8:0.2 TQ1:PCBM:PCBA (bottom) films annealed for 10 min at 140 °C

The thermal behaviour of the polymer:fullerene mixtures was investigated using differential scanning calorimetry (DSC). First heating thermograms of solution-cast neat TQ1:PCBM feature an endotherm with a peak at 272 °C and exotherm at 245 °C. For ternary blends containing 10 wt% PCBP or PCBA no transition could be distinguished. Based on this it is probable that PCBA and PCBP inhibits crystallization of PCBM, which in accordance with the absence of fullerene crystals seen in the SEM and AFM images of spin coated films.

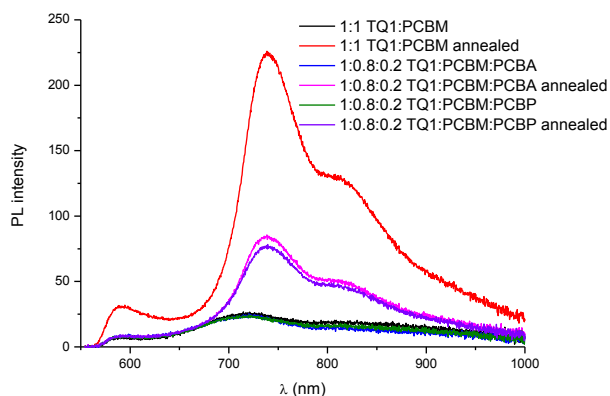


Figure 5.4: Photoluminescence spectra of TQ1:PCBM, TQ1:PCBM:PCBA and TQ1:PCBM:PCBP films before and after annealing at 140 °C for 10 min

## 5.4 Photovoltaic performance

The photovoltaic performance of TQ1:PCBM, TQ1:PCBM:PCBA and TQ1:PCBM:PCBP solar cells (Table 5.2) was investigated before and after annealing of the active layer. The polymer:fullerene ratio was kept constant at a 1:1 weight ratio. Standard devices of TQ1:PCBM using the same weight ratio have previously shown an efficiency of 3.5% in un-annealed devices. [96] Inverted devices with an architecture of glass/ITO/active layer/MoO<sub>3</sub>/Al were prepared by spin-coating active layers from 20 g L<sup>-1</sup> oDCB solutions on top of ITO. The active layer was then annealed at 140 °C for 15 min before evaporation of the metal electrodes. Due to the unsuitable work function of the ITO cathode, TQ1:PCBM devices show a very low V<sub>OC</sub> of 0.1-0.4 V resulting in a very low overall performance of 0.2 %. The improper conditions for the TQ1:PCBM devices is clearly visible by the shape of the corresponding IV-curves in Figure 5.5. In contrary, devices with PCBA and PCBP show decent V<sub>OC</sub> of 0.7-0.8 V and photovoltaic performance of 1-3 %. The improvement in V<sub>OC</sub> suggests that PCBA and PCBP alter the work function of ITO, resulting in a better matching of the electrode energy levels to the active material. Annealing of TQ1:PCBM devices

result in a major drop in  $J_{SC}$  from initial  $7.6 \text{ mA cm}^{-2}$  to  $< 1 \text{ mA cm}^{-2}$ . This is a result of formation of large PCBM crystals and phase separation of the blend resulting in a decreased polymer:fullerene interfacial area. Active layers of TQ1:PCBM:PCBA and TQ1:PCBM:PCBP on the other hand, retain their initial photocurrent and  $J_{SC}$  of  $5\text{-}9 \text{ mA cm}^{-2}$  after annealing as well as an increased FF. The increase in FF is likely due to an increased self-assembly of PCBA and PCBP molecules at the ITO interface upon annealing, resulting in a reduction of the undesired charge flow at the cathode interface. Concisely, TQ1:PCBM:PCBA and TQ1:PCBM:PCBP devices remain stable or even improve their photovoltaic performance after annealing at  $140 \text{ }^\circ\text{C}$ , whereas the efficiency of neat TQ1:PCBM devices is diminished by treatment at the same conditions. These differences in device performance are ascribed to the detrimental coarsening of the nanostructure as well as the growth of large PCBM crystals in TQ1:PCBM films. In contrast, the nanostructure of ternary blend films is preserved and, in addition, the ability of PCBA and PCBP to function as a self-assembling interlayer material provides a more favorable contact of the ITO-electrode.

*Table 5.2: Device performance initially and after annealing at  $140 \text{ }^\circ\text{C}$  for 15 min. Values are average over 4-6 cell, maximum attained PCE is shown in brackets*

Active layer blend	Annealing	$J_{SC}$ ( $\text{mA/cm}^2$ )	$V_{OC}$ (V)	FF (%)	PCE (%)
TQ1:PCBM		7.5	0.1	0.3	0.2 (0.3)
1:1	$140 \text{ }^\circ\text{C}$ , 15 min	0.6	0.2	0.6	0.04 (0.06)
TQ1:PCBM:PCBA		8.8	0.73	46	2.9 (3.3)
1:0.9:0.1	$140 \text{ }^\circ\text{C}$ , 15 min	6.7	0.65	49	2.1 (2.6)
TQ1:PCBM:PCBA		6.5	0.71	36	1.9 (2.2)
1:0.8:0.2	$140 \text{ }^\circ\text{C}$ , 15 min	4.9	0.78	48	1.7 (2.4)
TQ1:PCBM:PCBP		6.6	0.76	38	1.9 (2.5)
1:0.9:0.1	$140 \text{ }^\circ\text{C}$ , 15 min	5.2	0.69	51	1.8 (2.1)
TQ1:PCBM:PCBP		4.8	0.69	31	1.1 (1.3)
1:0.8:0.2	$140 \text{ }^\circ\text{C}$ , 15 min	3.8	0.75	49	1.3 (1.6)

## Fullerene Derivatives

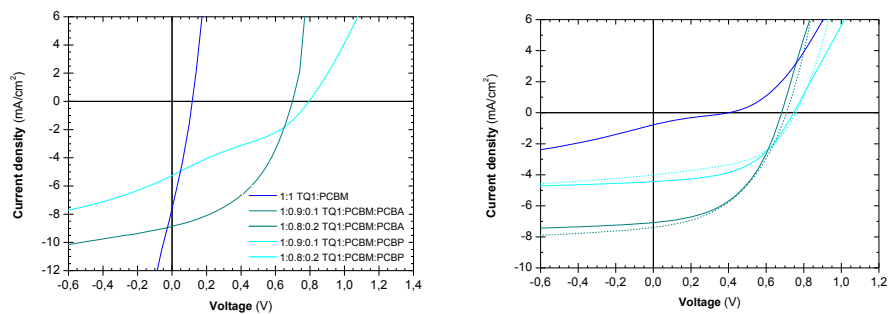


Figure 5.5: IV-curves of representative devices before (left) and after annealing (right)

## Fullerene Derivatives

## 6 CONCLUDING REMARKS

---

Polymer solar cells are a promising alternative to silicon-based solar cells due to their ease of production by large-area printing or coating techniques, which offer a potential for low cost, flexible devices. However, several issues must be resolved before the efficiencies of lab-scale devices can be reproduced. One critical aspect concerns the inverted geometry of large-area devices that typically require modification of the bottom electrode with interlayers in order to achieve high performance. The design, synthesis and evaluation of such interfacial materials have been the main subjects of this thesis.

In Chapter 3 the structure-property relationships for three DPP-based active layer polymers is investigated. Alkoxy substitution of the polymer influenced various properties, consistent with increased flexibility in the polymer chains. By comparing oligomer and polymer properties it is noticeable that they respond divergent to structural alterations due to conformational distribution that can arise in the polymer chain. The increase in HOMO-level for the alkoxy-substituted polymers together with a change in nanostructure of the BHJ blend seems to limit the photovoltaic performance of these polymers.

Inverted polymer solar cells have shown superior stability compared to devices with conventional architecture. However, a low performance is often seen due to limitations at the active layer/electrode interface. One approach to overcome this problem is to use an interlayer material to modify the interface between the cathode and the active layer. Four different polymer interlayers were presented in Chapter 4. In the first part of the chapter, highly efficient ITO-free inverted solar cells were investigated using an ultrathin interlayer of PFPA-1 between the  $\text{TiO}_x/\text{Al}$  cathode and the active layer. The performance of devices was improved from 3.7% to 5.2% when using the PFPA-1 interlayer polymer. In addition, PFPA-1 altered the surface energy of the cathode, leading to the formation of a finer morphology upon deposition of the active layer and an improvement in  $J_{\text{SC}}$ . Furthermore, the hole-blocking ability of PFPA-1 contributed to an increase in FF.

## Concluding remarks

In the second part of Chapter 4, PFFA-1 is compared to three similar polymers where the fluorene monomer has been exchanged with monomers that have been reported to have a higher photo-chemical stability. The polymer interlayers were studied in terms of their influence on device performance and stability on inverted devices with an active layer of P3HT:PC<sub>61</sub>BM. The use of the different interlayers increase the PCE of devices with 50% compared to devices without interlayer and also improves the stability of the inverted solar cells. The effect is mainly due to improved  $V_{oc}$  and FF, originating from the interlayers' ability to reduce the undesired charge collection at the cathode interface as well as to provide better energy level alignment. The results indicate that the use of an interlayer in general improves the stability and performance of the solar cells. It would be interesting to look in to the possibility of incorporating a polymer interlayer at the anode. A selective anode could potentially further increase both FF and  $V_{oc}$ .

Unfortunately, many interlayer materials have shown low air stability and in addition, the deposition of the interlayer introduces an additional step to the production process. A self-assembly approach can be employed to circumvent these problems. Furthermore, the roll-to-roll process usually involves several heating steps in order to achieve rapid solvent removal. It is therefore crucial that the polymer:fullerene blend nanostructure is thermally stable at these conditions. In Chapter 5, two fullerene derivatives, PCBA and PCBP, were used to simultaneously achieve both work function modification of the electrode and improved thermal stability of a polymer:fullerene bulk-heterojunction blend. The use of the fullerene interlayers resulted in higher photovoltaic performance of the inverted solar cells. Moreover, the photovoltaic performance is retained in polymer solar cell blends that otherwise rapidly deteriorates at elevated temperatures. In particular, fullerene crystallization in devices that contain PCBA or PCBP is hindered at annealing temperatures that are suitable for roll-to-roll processes. A possible continuation of this study could be to look in to different PCBM modifications and combinations thereof to potentially be able to better control the bulk nanostructure and electrode

## Concluding remarks

work function in PSCs. It would also be interesting to try this concept using a functionalized derivative of the active layer polymer as a self-assembling interlayer.

The work presented in this thesis is anticipated to be applicable to a wide range of polymer:fullerene systems and thereby provide valuable information for the further development of PSCs.

## Concluding remarks

## ACKNOWLEDGEMENTS

---

Mats R. Andersson, for accepting me as a PhD student and for the guidance and support during my years at Chalmers.

Christian Müller, for adopting me into your group and for all your encouragement and help. I have really enjoyed being a part of your group.

My co-authors of the papers included in this thesis for all your contributions and help.

All former and present co-workers at floor 8. Especially I would like to thank Camilla Johansson, Sofie Gårdebjer, Markus Jarvid and Mattan Andersson for being such great friends. To all the people in the “fika team” (you know who you are) thank you for all discussions and laughter. Patrik Henriksson and Zhaojun Li for being the best office roommates. Renee Kroon, Tim Steckler, Camilla Johansson, Amaia Diaz de Zerio Mendaza and Sandra Fusco for all the help and discussions in the lab and for all the fun conference trips.

Frida Andersson, Lotta Pettersson, Carina Pettersson, Anne Wendel, Ann Jakobsson, Anders Mårtensson and Roger Forsman for all your help and for making everything run smoothly at Applied Chemistry.

Friends and family for all your support and encouragement.

Marcus and Henry for all your love and support. You always remind me of what is important, I would not have made it without you.

## Acknowledgements

## REFERENCES

---

- [1] European Commission, [http://ec.europa.eu/clima/policies/brief/causes/index\\_en.htm](http://ec.europa.eu/clima/policies/brief/causes/index_en.htm), 141022
- [2] EIA, International Energy Statistics, in, 2014.
- [3] Martin A. Green, Keith Emery, Yoshihiro Hishikawa, Wilhelm Warta, Ewan D. Dunlop, Progress in Photovoltaics: Research and Applications, 23 (2015) 1-9.
- [4] Hideki Shirakawa, Edwin J. Louis, Alan G. MacDiarmid, Chwan K. Chiang, Alan J. Heeger, Journal of the Chemical Society, Chemical Communications, (1977) 578-580.
- [5] Nobel Media AB, [http://www.nobelprize.org/nobel\\_prizes/chemistry/laureates/2000/](http://www.nobelprize.org/nobel_prizes/chemistry/laureates/2000/), The Nobel Prize in Chemistry 2000, 141022
- [6] Zhicai He, Chengmei Zhong, Shijian Su, Miao Xu, Hongbin Wu, Yong Cao, Nature Photonics, 6 (2012) 591-595.
- [7] Sih-Hao Liao, Hong-Jyun Jhuo, Yu-Shan Cheng, Show-An Chen, Advanced Materials, 25 (2013) 4766-4771.
- [8] Yuhang Liu, Jingbo Zhao, Zhengke Li, Cheng Mu, Wei Ma, Huawei Hu, Kui Jiang, Haoran Lin, Harald Ade, He Yan, Nature Communications, 5 (2014).
- [9] William Shockley, Hans J. Queisser, Journal of Applied Physics, 32 (1961) 510-519.
- [10] Christoph J. Brabec, Srinivas Gowrisanker, Jonathan J. M. Halls, Darin Laird, Shijun Jia, Shawn P. Williams, Advanced Materials, 22 (2010) 3839-3856.
- [11] Nobel Media AB 2014, [http://www.nobelprize.org/nobel\\_prizes/chemistry/laureates/2000/shirakawa-lecture.html](http://www.nobelprize.org/nobel_prizes/chemistry/laureates/2000/shirakawa-lecture.html), Hideki Shirakawa - Nobel Lecture: The Discovery of Polyacetylene Film: The Dawning of an Era of Conducting Polymers, 141021
- [12] Frederik C. Krebs, Solar Energy Materials and Solar Cells, 93 (2009) 394-412.
- [13] Roar Søndergaard, Markus Hösel, Dechan Angmo, Thue T. Larsen-Olsen, Frederik C. Krebs, Materials Today, 15 (2012) 36-49.
- [14] Meng Wang, Gui-Zhong Yang, Min Wang, Tianxi Liu, Polymers for Advanced Technologies, 21 (2010) 381-385.
- [15] E. E. Havinga, W. ten Hoeve, H. Wynberg, Polymer Bulletin, 29 (1992) 119-126.
- [16] Jan C. Hummelen, Brian W. Knight, F. LePeq, Fred Wudl, Jie Yao, Charles L. Wilkins, The Journal of Organic Chemistry, 60 (1995) 532-538.
- [17] Martijn M. Wienk, Jan M. Kroon, Wiljan J. H. Verhees, Joop Knol, Jan C. Hummelen, Paul A. van Hal, René A. J. Janssen, Angewandte Chemie International Edition, 42 (2003) 3371-3375.
- [18] Sabine Bertho, Ilse Haeldermans, Ann Swinnen, Wouter Moons, Tom Martens, Laurence Lutsen, Dirk Vanderzande, Jean Manca, Alessia Senes, Annalisa Bonfiglio, Solar Energy Materials and Solar Cells, 91 (2007) 385-389.
- [19] Bert Conings, Sabine Bertho, Koen Vandewal, Alessia Senes, Jan D'Haen, Jean Manca, René A. J. Janssen, Applied Physics Letters, 96 (2010) -.

## References

- [20] Jonas Bergqvist, Camilla Lindqvist, Olof Backe, Zaifei Ma, Zheng Tang, Wolfgang Tress, Stefan Gustafsson, Ergang Wang, Eva Olsson, Mats R. Andersson, Olle Inganäs, Christian Muller, *Journal of Materials Chemistry A*, 2 (2014) 6146-6152.
- [21] B. R. Weinberger, M. Akhtar, S. C. Gau, *Synthetic Metals*, 4 (1982) 187-197.
- [22] C. W. Tang, *Applied Physics Letters*, 48 (1986) 183-185.
- [23] N. S. Sariciftci, D. Braun, C. Zhang, V. I. Srdanov, A. J. Heeger, G. Stucky, F. Wudl, *Applied Physics Letters*, 62 (1993) 585-587.
- [24] J. J. M. Halls, C. A. Walsh, N. C. Greenham, E. A. Marseglia, R. H. Friend, S. C. Moratti, A. B. Holmes, *Nature*, 376 (1995) 498-500.
- [25] G. Yu, J. Gao, J. C. Hummelen, F. Wudl, A. J. Heeger, *Science*, 270 (1995) 1789-1791.
- [26] Th Kugler, W. R. Salaneck, H. Rost, A. B. Holmes, *Chemical Physics Letters*, 310 (1999) 391-396.
- [27] Christoph J. Brabec, Sean E. Shaheen, Christoph Winder, N. Serdar Sariciftci, Patrick Denk, *Applied Physics Letters*, 80 (2002) 1288-1290.
- [28] Chih-Ping Chen, Yeu-Ding Chen, Shih-Ching Chuang, *Advanced Materials*, 23 (2011) 3859-3863.
- [29] Jacek J. Jasieniak, Jason Seifter, Jang Jo, Tom Mates, Alan J. Heeger, *Advanced Functional Materials*, 22 (2012) 2594-2605.
- [30] Tobias Nyberg, *Synthetic Metals*, 140 (2004) 281-286.
- [31] M. Glatthaar, M. Niggemann, B. Zimmermann, P. Lewer, M. Riede, A. Hinsch, J. Luther, *Thin Solid Films*, 491 (2005) 298-300.
- [32] B. Zimmermann, M. Glatthaar, M. Niggemann, M. K. Riede, A. Hinsch, A. Gombert, *Solar Energy Materials and Solar Cells*, 91 (2007) 374-378.
- [33] B. Zimmermann, U. Würfel, M. Niggemann, *Solar Energy Materials and Solar Cells*, 93 (2009) 491-496.
- [34] Matthieu Manceau, Dechan Angmo, Mikkel Jørgensen, Frederik C. Krebs, *Organic Electronics*, 12 (2011) 566-574.
- [35] Brian Azzopardi, Christopher J. M. Emmott, Antonio Urbina, Frederik C. Krebs, Joseph Mutale, Jenny Nelson, *Energy & Environmental Science*, 4 (2011) 3741-3753.
- [36] J. J. M. Halls, K. Pichler, R. H. Friend, S. C. Moratti, A. B. Holmes, *Applied Physics Letters*, 68 (1996) 3120-3122.
- [37] Leif A. A. Pettersson, Lucimara S. Roman, Olle Inganäs, *Journal of Applied Physics*, 86 (1999) 487-496.
- [38] M. Theander, A. Yartsev, D. Zigmantas, V. Sundström, W. Mammo, M. R. Andersson, O. Inganäs, *Physical Review B*, 61 (2000) 12957-12963.
- [39] J. J. M. Halls, J. Cornil, D. A. dos Santos, R. Silbey, D. H. Hwang, A. B. Holmes, J. L. Brédas, R. H. Friend, *Physical Review B*, 60 (1999) 5721-5727.
- [40] Jean-Luc Brédas, David Beljonne, Veaceslav Coropceanu, Jérôme Cornil, *Chemical Reviews*, 104 (2004) 4971-5004.
- [41] F. Zhang, K. G Jespersen, C. Björström, M. Svensson, M. R Andersson, V. Sundström, K. Magnusson, E. Moons, A. Yartsev, O. Inganäs, *Advanced Functional Materials*, 16 (2006) 667-674.

## References

- [42] Koen Vandewal, Kristofer Tvingstedt, Abay Gadisa, Olle Inganäs, Jean V. Manca, *Nat Mater*, 8 (2009) 904-909.
- [43] Yen-Ju Cheng, Tien-Yau Luh, *Journal of Organometallic Chemistry*, 689 (2004) 4137-4148.
- [44] Norio Miyaura, Akira Suzuki, *Chemical Reviews*, 95 (1995) 2457-2483.
- [45] John K. Stille, *Angewandte Chemie International Edition in English*, 25 (1986) 508-524.
- [46] Nobel Media AB, [http://www.nobelprize.org/nobel\\_prizes/chemistry/laureates/2010/](http://www.nobelprize.org/nobel_prizes/chemistry/laureates/2010/), The Nobel Prize in Chemistry 2010, 141022
- [47] Ivan J. Boyer, *Toxicology*, 55 (1989) 253-298.
- [48] J. Mizuguchi, A. Grubenmann, G. Wooden, G. Rihs, *Acta Crystallographica Section B*, 48 (1992) 696-700.
- [49] Daniel A. M. Egbe, Stefan Türk, Silke Rathgeber, Florian Kühnlenz, Rupali Jadhav, Andreas Wild, Eckhard Birkner, Getachew Adam, Almantas Pivrikas, Vera Cimrova, Günther Knör, Niyazi S. Sariciftci, Harald Hoppe, *Macromolecules*, 43 (2010) 1261-1269.
- [50] Marie-France Falzon, Arjan P. Zoombelt, Martijn M. Wienk, René A. J. Janssen, *Physical Chemistry Chemical Physics*, 13 (2011) 8931-8939.
- [51] Erjun Zhou, Shimpei Yamakawa, Keisuke Tajima, Chunhe Yang, Kazuhito Hashimoto, *Chemistry of Materials*, 21 (2009) 4055-4061.
- [52] Thomas Beyerlein, Bernd Tieke, *Macromolecular Rapid Communications*, 21 (2000) 182-189.
- [53] Johan C. Bijleveld, Veronique S. Gevaerts, Daniele Di Nuzzo, Mathieu Turbiez, Simon G. J. Mathijssen, Dago M. de Leeuw, Martijn M. Wienk, René A. J. Janssen, *Advanced Materials*, 22 (2010) E242-E246.
- [54] Yongye Liang, Danqin Feng, Yue Wu, Szu-Ting Tsai, Gang Li, Claire Ray, Luping Yu, *Journal of the American Chemical Society*, 131 (2009) 7792-7799.
- [55] H. A. M. van Mullekom, J. A. J. M. Vekemans, E. E. Havinga, E. W. Meijer, *Materials Science and Engineering: R: Reports*, 32 (2001) 1-40.
- [56] M. C Scharber, D. Mühlbacher, M. Koppe, P. Denk, C. Waldauf, A. J Heeger, C. J Brabec, *Advanced Materials*, 18 (2006) 789-794.
- [57] Martijn M. Wienk, Mathieu Turbiez, Jan Gilot, René A. J. Janssen, *Advanced Materials*, 20 (2008) 2556-2560.
- [58] T. Ishida, H. Kobayashi, Y. Nakato, *Journal of Applied Physics*, 73 (1993) 4344-4350.
- [59] J. Shewchun, J. Dubow, C. W. Wilmsen, R. Singh, D. Burk, J. F. Wager, *Journal of Applied Physics*, 50 (1979) 2832-2839.
- [60] I. D. Parker, *Journal of Applied Physics*, 75 (1994) 1656-1666.
- [61] Y. Park, V. Choong, Y. Gao, B. R. Hsieh, C. W. Tang, *Applied Physics Letters*, 68 (1996) 2699-2701.
- [62] Xavier Bulliard, Soo-Ghang Ihn, Sungyoung Yun, Yungi Kim, Dukhyun Choi, Jae-Young Choi, Min Kim, Myungsun Sim, Jong-Hwan Park, Woong Choi, Kilwon Cho, *Advanced Functional Materials*, 20 (2010) 4381-4387.
- [63] Jie Luo, Hongbin Wu, Chao He, Aiyuan Li, Wei Yang, Yong Cao, *Applied Physics Letters*, 95 (2009).

## References

- [64] Chao He, Chengmei Zhong, Hongbin Wu, Renqiang Yang, Wei Yang, Fei Huang, Guillermo C. Bazan, Yong Cao, *Journal of Materials Chemistry*, 20 (2010) 2617-2622.
- [65] Jung Hwa Seo, Andrea Gutacker, Yanming Sun, Hongbin Wu, Fei Huang, Yong Cao, Ullrich Scherf, Alan J. Heeger, Guillermo C. Bazan, *Journal of the American Chemical Society*, 133 (2011) 8416-8419.
- [66] Yinhua Zhou, Canek Fuentes-Hernandez, Jaewon Shim, Jens Meyer, Anthony J. Giordano, Hong Li, Paul Winget, Theodoros Papadopoulos, Hyeunseok Cheun, Jungbae Kim, Mathieu Fenoll, Amir Dindar, Wojciech Haske, Ehsan Najafabadi, Talha M. Khan, Hossein Sojoudi, Stephen Barlow, Samuel Graham, Jean-Luc Brédas, Seth R. Marder, Antoine Kahn, Bernard Kippelen, *Science*, 336 (2012) 327-332.
- [67] Yongxiang Zhu, Xiaofeng Xu, Lianjie Zhang, Junwu Chen, Yong Cao, *Solar Energy Materials and Solar Cells*, 97 (2012) 83-88.
- [68] Maxime Ranger, Mario Leclerc, *Macromolecules*, 32 (1999) 3306-3313.
- [69] L. J. Lindgren, X. Wang, O. Inganäs, M. R. Andersson, *Synthetic Metals*, 154 (2005) 97-100.
- [70] Ergang Wang, Lintao Hou, Zhongqiang Wang, Stefan Hellström, Fengling Zhang, Olle Inganäs, Mats R. Andersson, *Advanced Materials*, 22 (2010) 5240-5244.
- [71] Cecilia M. Björström, Svante Nilsson, Andrzej Bernasik, Andrzej Budkowski, Mats Andersson, Kjell O. Magnusson, Ellen Moons, *Applied Surface Science*, 253 (2007) 3906-3912.
- [72] Yousuke Ooyama, Shogo Inoue, Tomoya Nagano, Kohei Kushimoto, Joji Ohshita, Ichiro Imae, Kenji Komaguchi, Yutaka Harima, *Angewandte Chemie International Edition*, 50 (2011) 7429-7433.
- [73] Mikkel Jørgensen, Kion Norrman, Frederik C. Krebs, *Solar Energy Materials and Solar Cells*, 92 (2008) 686-714.
- [74] Yücel Şahin, Salima Alem, Rémi de Bettignies, Jean-Michel Nunzi, *Thin Solid Films*, 476 (2005) 340-343.
- [75] A. Hadipour, R. Müller, P. Heremans, *Organic Electronics*, 14 (2013) 2379-2386.
- [76] Matthieu Manceau, Eva Bundgaard, Jon E. Carle, Ole Hagemann, Martin Helgesen, Roar Sondergaard, Mikkel Jørgensen, Frederik C. Krebs, *Journal of Materials Chemistry*, 21 (2011) 4132-4141.
- [77] Mikkel Jørgensen, Kion Norrman, Suren A. Gevorgyan, Thomas Tromholt, Birgitta Andreasen, Frederik C. Krebs, *Advanced Materials*, 24 (2012) 580-612.
- [78] Matthew O. Reese, Suren A. Gevorgyan, Mikkel Jørgensen, Eva Bundgaard, Sarah R. Kurtz, David S. Ginley, Dana C. Olson, Matthew T. Lloyd, Pasquale Morvillo, Eugene A. Katz, Andreas Elschner, Olivier Haillant, Travis R. Currier, Vishal Shrotriya, Martin Hermenau, Moritz Riede, Kiril R. Kirov, Gregor Trimmel, Thomas Rath, Olle Inganäs, Fengling Zhang, Mattias Andersson, Kristofer Tvingstedt, Monica Lira-Cantu, Darin Laird, Christine McGuinness, Srinivas Gowrisanker, Michael Pannone, Min Xiao, Jens Hauch, Roland Steim, Dean M. DeLongchamp, Roland Rösch, Harald Hoppe, Nieves Espinosa, Antonio Urbina, Gülsah Yaman-Uzunoglu, Jörg-Bernd Bonekamp, Albert J. J. M. van Breemen,

## References

- Claudio Girotto, Eszter Voroshazi, Frederik C. Krebs, *Solar Energy Materials and Solar Cells*, 95 (2011) 1253-1267.
- [79] Stefan Schäfer, Andreas Petersen, Thomas A. Wagner, Rolf Kniprath, Dominic Lingenfelder, Achmad Zen, Thomas Kirchartz, Birger Zimmermann, Uli Würfel, Xianjin Feng, Thomas Mayer, *Physical Review B*, 83 (2011) 165311.
- [80] S. Khelifi, E. Voroshazi, D. Spoltore, F. Piersimoni, S. Bertho, T. Aernouts, J. Manca, J. Lauwaert, H. Vrielinck, M. Burgelman, *Solar Energy Materials and Solar Cells*, 120, Part A (2014) 244-252.
- [81] Sarah R. Cowan, Philip Schulz, Anthony J. Giordano, Andres Garcia, Bradley A. MacLeod, Seth R. Marder, Antoine Kahn, David S. Ginley, Erin L. Ratcliff, Dana C. Olson, *Advanced Functional Materials*, 24 (2014) 4671-4680.
- [82] Bertram Heinz, Harald Morgner, *Journal of Electron Spectroscopy and Related Phenomena*, 96 (1998) 83-95.
- [83] S. Gutmann, M. Conrad, M. A. Wolak, M. M. Beerbom, R. Schlaf, *Journal of Applied Physics*, 111 (2012) 123710.
- [84] Di Ma, Menglan Lv, Ming Lei, Jin Zhu, Haiqiao Wang, Xiwen Chen, *ACS Nano*, 8 (2014) 1601-1608.
- [85] Frederik C. Krebs, *Solar Energy Materials and Solar Cells*, 93 (2009).
- [86] Sabine Bertho, Griet Janssen, Thomas J. Cleij, Bert Conings, Wouter Moons, Abay Gadisa, Jan D'Haen, Etienne Goovaerts, Laurence Lutsen, Jean Manca, Dirk Vanderzande, *Solar Energy Materials and Solar Cells*, 92 (2008) 753-760.
- [87] Christian Muller, Jonas Bergqvist, Koen Vandewal, Kristofer Tvingstedt, Ana Sofia Anselmo, Roger Magnusson, M. Isabel Alonso, Ellen Moons, Hans Arwin, Mariano Campoy-Quiles, Olle Inganäs, *Journal of Materials Chemistry*, 21 (2011) 10676-10684.
- [88] Xiaoni Yang, Jeroen K. J. van Duren, René A. J. Janssen, Matthias A. J. Michels, Joachim Loos, *Macromolecules*, 37 (2004) 2151-2158.
- [89] Camilla Lindqvist, Anke Sanz-Velasco, Ergang Wang, Olof Backe, Stefan Gustafsson, Eva Olsson, Mats R. Andersson, Christian Muller, *Journal of Materials Chemistry A*, 1 (2013) 7174-7180.
- [90] Hung-Wei Liu, Deng-Yang Chang, Wen-Yen Chiu, Syang-Peng Rwei, Leeyih Wang, *Journal of Materials Chemistry*, 22 (2012) 15586-15591.
- [91] Charn-Ying Chen, Cheng-Si Tsao, Yu-Ching Huang, Hung-Wei Liu, Wen-Yen Chiu, Chih-Min Chuang, U. Ser Jeng, Chun-Jen Su, Wei-Ru Wu, Wei-Fang Su, Leeyih Wang, *Nanoscale*, 5 (2013) 7629-7638.
- [92] Bob C. Schroeder, Zhe Li, Michael A. Brady, Gregório Couto Faria, Raja Shahid Ashraf, Christopher J. Takacs, John S. Cowart, Duc T. Duong, Kar Ho Chiu, Ching-Hong Tan, João T. Cabral, Alberto Salleo, Michael L. Chabiny, James R. Durrant, Iain McCulloch, *Angewandte Chemie International Edition*, 53 (2014) 12870-12875.
- [93] Yoshihide Santo, Il Jeon, Kee Sheng Yeo, Takafumi Nakagawa, Yutaka Matsuo, *Applied Physics Letters*, 103 (2013) -.
- [94] Camilla Lindqvist, Jonas Bergqvist, Olof Bäcké, Stefan Gustafsson, Ergang Wang, Eva Olsson, Olle Inganäs, Mats R. Andersson, Christian Müller, *Applied Physics Letters*, 104 (2014) 153301.

## References

- [95] Jeffrey J. Richards, Andrew H. Rice, Rainie D. Nelson, Felix S. Kim, Samson A. Jenekhe, Christine K. Luscombe, Danilo C. Pozzo, *Advanced Functional Materials*, 23 (2013) 514-522.
- [96] Camilla Lindqvist, Jonas Bergqvist, Ching-Chiao Feng, Stefan Gustafsson, Olof Bäcke, Neil D. Treat, Céline Bounioux, Patrik Henriksson, Renee Kroon, Ergang Wang, Anke Sanz-Velasco, Per Magnus Kristiansen, Natalie Stingelin, Eva Olsson, Olle Inganäs, Mats R. Andersson, Christian Müller, *Advanced Energy Materials*, 4 (2014) n/a-n/a.
- [97] Zheng Tang, Wolfgang Tress, Qinye Bao, Mohammad J. Jafari, Jonas Bergqvist, Thomas Ederth, Mats R. Andersson, Olle Inganäs, *Advanced Energy Materials*, 4 (2014) n/a-n/a.
- [98] Ari Laiho, Robin H. A. Ras, Sami Valkama, Janne Ruokolainen, Ronald Österbacka, Olli Ikkala, *Macromolecules*, 39 (2006) 7648-7653.
- [99] Zhe Li, Him Cheng Wong, Zhenggang Huang, Hongliang Zhong, Ching Hong Tan, Wing Chung Tsoi, Ji Seon Kim, James R. Durrant, João T. Cabral, *Nat Commun*, 4 (2013).